Cell Reports

Article

Not4 and Not5 modulate translation elongation by Rps7A ubiquitination, Rli1 moonlighting, and condensates that exclude eIF5A

Graphical abstract

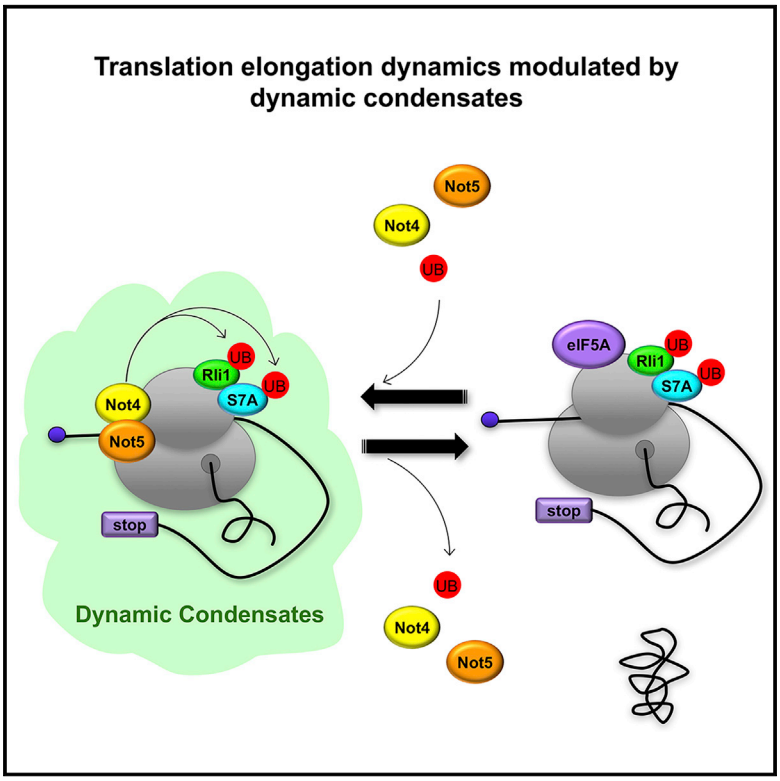

Authors

George E. Allen, Olesya O. Panasenko, Zoltan Villanyi, ..., Vicent Pelechano, Zoya Ignatova, Martine A. Collart

Correspondence

martine.collart@unige.ch

In brief

Allen et al. show that codon-specific translation elongation dynamics are modulated by Not4 and Not5, in coordination with Rli1 and opposing eIF5A function, and according to codon optimality to produce a soluble proteome. We propose that this regulation occurs by dynamic condensates that limit mRNA solubility and exclude eIF5A.

Highlights

- Not subunits of the Ccr4-Not complex form dynamic condensates excluding eIF5A
- In *not*Δ cells, ribosome dwelling occupancies change according to codon optimality
- Ribosome dwelling inversely changes upon eIF5A depletion and Not deletion
- Rli1 moonlighting and Rps7A ubiquitination contribute to Not regulation

Allen et al., 2021, Cell Reports *36*, 109633
August 31, 2021
https://doi.org/10.1016/j.celrep.2021.109633

CellPress

Cell Reports

CellPress
OPEN ACCESS

Article

Not4 and Not5 modulate translation elongation by Rps7A ubiquitination, Rli1 moonlighting, and condensates that exclude eIF5A

George E. Allen,[1,6] Olesya O. Panasenko,[1,6] Zoltan Villanyi,[1,2] Marina Zagatti,[1] Benjamin Weiss,[1] Lucile Pagliazzo,[1] Susanne Huch,[3] Christine Polte,[4] Szabolcs Zahoran,[1,2] Christopher S. Hughes,[5] Vicent Pelechano,[3] Zoya Ignatova,[4] and Martine A. Collart[1,7,*]

[1]Department of Microbiology and Molecular Medicine, Institute of Genetics and Genomics Geneva, Faculty of Medicine, University of Geneva, 1211 Geneva 4, Switzerland
[2]Department of Biochemistry and Molecular Biology, Faculty of Science and Informatics, University of Szeged, 6726 Szeged, Hungary
[3]SciLifeLab, Department of Microbiology, Tumor and Cell Biology, Karolinska Institutet, 17165 Solna, Sweden
[4]Institute of Biochemistry and Molecular Biology, University of Hamburg, 20146 Hamburg, Germany
[5]Department of Molecular Oncology, BC Cancer, Vancouver, BC V5Z1L3, Canada
[6]These authors contributed equally
[7]Lead contact
*Correspondence: martine.collart@unige.ch
https://doi.org/10.1016/j.celrep.2021.109633

SUMMARY

In this work, we show that Not4 and Not5 from the Ccr4-Not complex modulate translation elongation dynamics and change ribosome A-site dwelling occupancy in a codon-dependent fashion. These codon-specific changes in *not5Δ* cells are very robust and independent of codon position within the mRNA, the overall mRNA codon composition, or changes of mRNA expression levels. They inversely correlate with codon-specific changes in cells depleted for eIF5A and positively correlate with those in cells depleted for ribosome-recycling factor Rli1. Not5 resides in punctate loci, co-purifies with ribosomes and Rli1, but not with eIF5A, and limits mRNA solubility. Overexpression of wild-type or non-complementing Rli1 and loss of Rps7A ubiquitination enable Not4 E3 ligase-dependent translation of polyarginine stretches. We propose that Not4 and Not5 modulate translation elongation dynamics to produce a soluble proteome by Rps7A ubiquitination, dynamic condensates that limit mRNA solubility and exclude eIF5A, and a moonlighting function of Rli1.

INTRODUCTION

The Ccr4-Not complex is a global regulator of mRNA metabolism in eukaryotic cells (for review see Collart, 2016). It regulates transcription and RNA quality control in the nucleus (Azzouz et al., 2009a; Kruk et al., 2011; Reese, 2013) and represses gene expression in the cytoplasm (Rouya et al., 2014; Sandler et al., 2011). Ccr4-Not also plays an important role in co-translational processes (Kassem et al., 2017; Villanyi et al., 2014). Not1, the largest subunit, can assemble in granules, named assemblysomes, which protect stalled ribosomes from the ribosome quality control (RQC) machinery and enable co-translational association of proteins (Panasenko et al., 2019). Not5 facilitates the translation of transcripts encoding ribosomal proteins (RPs), likely through a process that involves Not1-mediated mRNA binding (Gupta et al., 2016). The Not4 RING E3 ligase ubiquitinates the Rps7A RP (Panasenko and Collart, 2012) and the ribosome-associated chaperone NAC (Panasenko et al., 2006). Not4 is a relevant player in non-canonical RQC and No-Go-Decay (NGD) that occurs when ribosomes stall during translation, at least by its ubiquitination of Rps7A (Ikeuchi et al., 2019). RQC-induced ribosome splitting requires Rli1, an ATP-binding protein that directly binds the ribosome in the inter-subunit space, at the GTPase binding center. It is a key ribosome-recycling factor (Young et al., 2015). For translation termination, Rli1 couples peptide release and ribosome splitting, in collaboration with termination factors or with the ribosome rescue factor Dom34 (Guydosh and Green, 2014). It also promotes pre-initiation complex assembly (Dong et al., 2004).

A direct interaction of Not5 with the ribosome was recently shown structurally in a complex purified by Not4; the N-terminal domain of Not5 interacts with the ribosomal E site, which is the exit site of the deacylated tRNA. When Not4 was purified from monosome fractions, Not5 was found associated with late-initiation complexes, bearing the AUG codon and the initiator $tRNAi^{Met}$ in the peptidyl-tRNA binding site (P site) of the ribosome. In polysome fractions, Not5 engaged with ribosomes lacking a tRNA in the ribosomal A site, where incoming aminoacyl-tRNAs engage with the ribosome. Not5-associated ribosomes are in a post-translocation state and likely trap the ribosomes upon slow decoding of non-optimal A site codons (Buschauer et al., 2020). These structural findings suggest that ribosome association of Not5 and of eIF5A, which binds pre-translocation ribosomes, would be

mutually exclusive. eIF5A participates in the formation of the first peptide bond and stimulates methionyl-puromycin synthesis (Benne and Hershey, 1978) but otherwise is a dispensable factor for elongation. It binds stalled ribosomes with a vacant E site and facilitates the elongation of ribosomes paused at polyproline stretches and multiple other difficult-to-translate tripeptides (Schuller et al., 2017). Depletion of eIF5A also results in an accumulation of ribosomes at stop codons (Pelechano and Alepuz, 2017).

Structural work proposes that Not5 ribosome binding mediates Ccr4-Not monitoring of the translating ribosome for codon optimality and coordination with mRNA decay (Buschauer et al., 2020). Many other studies link mRNA turnover with the Ccr4-Not complex (e.g., Daugeron et al., 2001; Sandler et al., 2011; Stowell et al., 2016; Tucker et al., 2001). A massive aggregation of new proteins in cells when Not4 or Not5 are deleted supports their role in translation elongation (Halter et al., 2014; Panasenko and Collart, 2012; Preissler et al., 2015). Yet, the possible roles of Not4 and Not5 in translation dynamics and the mechanism of their action in translation remain elusive. In this work, we determined by means of ribosome profiling (Ribo-Seq) coupled to biochemical experiments that Not4 and Not5 cooperate in regulating translation elongation dynamics, in a mechanism that involves Rps7A ubiquitination, an Rli1 moonlighting function, and condensation of translating mRNAs that limit their access to eIF5A.

RESULTS

Not4 affects translation initiation, whereas Not5 facilitates both initiation and elongation

To characterize the global effect of Not4 and Not5 in translation, we first performed a genome-wide analysis by using RiboSeq in Not4-deleted (*not4Δ*) and Not5-deleted (*not5Δ*) strains and compared the profiles to wild-type (WT) yeast (Panasenko et al., 2019) under permissive growth conditions in glucose-rich medium. In total, 5,048 transcripts were detected as genuinely translated above the threshold (>1 reads per kilobase per million of sequencing reads [RPKMs]; Table S1), with very good reproducibility between biological replicates (Figure S1A), well-defined three-nucleotide periodicity (Figure S1B), and the majority of ribosome protected fragment (RPF) lengths between 28 and 31 nucleotides (Figure S1C).

Metagene analysis of RPFs across transcripts (Schuller et al., 2017) in *not4Δ* showed a significant RPF accumulation at the start codon with no effect on elongation (Figure 1A, top panel). In *not5Δ*, along with the increased RPFs at start, we observed a marked RPF increase within the first 100 codons of the coding sequences (CDSs), followed by a relaxation of the RPF coverage relative to that of the WT (Figure 1A, bottom panel). This difference in the metagene profile was due to transcripts with high overall RKPMs (those above median RPKM, referred to hereafter as highly expressed). In *not5Δ,* they exhibited higher amounts of RPFs accumulating within the 5′ vicinity of the CDSs (i.e., first CDS half) relative to the 3′ end of the CDS (i.e., second half). In contrast, the RPF distribution along the transcripts with overall lower RPKMs (those below median RPKM, referred to hereafter as lowly expressed) remained unchanged between first and second halves (Figure 1B).

Changes in RPFs correlate well with changes in *de novo* protein synthesis in *not5Δ*

We determined how well the overall changes in RPFs measured in mutants relative to WT reflected changes in new protein synthesis defined by SILAC analyses. For *not5Δ*, we used our published SILAC analysis (Gupta et al., 2016). This comparison revealed an overall good correlation (Figure 1C). For *not4Δ*, we performed a SILAC analysis with WT and *not4Δ* cells and evaluated changes (Table S1). Despite the overall good correlation, it was lower than that for *not5Δ* (Figure 1D). We noticed that the production of certain RPs and translation elongation factors was increased in *not4Δ* relative to WT, but RPFs for the mRNAs encoding these proteins were lower in the mutant than in the WT. Conversely, proteins involved in stress responses, the cell wall, and metabolism showed higher RPFs in *not4Δ* but remained unchanged in the SILAC measurement (Table S1).

Newly synthesized proteins aggregate massively in cells lacking Not5 or Not4 (Halter et al., 2014; Panasenko and Collart, 2012; Preissler et al., 2015). Proteomic analysis of the aggregates in *not5Δ* revealed that out of the detected 192 proteins (threshold of $\geq$2 peptides; Table S1), 143 were unique and absent in aggregates of WT cells. Of those proteins, 69.9% ($p = 2.2 \times 10^{-16}$, Fisher's exact test; Table S1) aggregated in cells lacking the ribosome-associated Ssb chaperone (Willmund et al., 2013). Proteins detected in the *not5Δ* aggregates were both from mRNAs with overall up- and downregulated RPFs and from highly expressed mRNAs (Figure S1D) known to be enriched for optimal codons. Proteins aggregating in *not4Δ* have been previously identified (Preissler et al., 2015). They were not particularly restricted to highly expressed mRNAs (Figure S1E) but were significantly enriched for mRNAs with greater increases of *de-novo*-produced proteins than RPF changes between the mutant and the WT (Figure 1D). There was an overall overlap of mRNA families whose translation was downregulated in both mutants (Figures S1F–S1I).

These experiments were performed with deletion mutants enabling detection of both direct and indirect consequences of Not4 and Not5 loss. Indeed, in *not5Δ*, besides RPs, the translation of several translation factors (e.g., Efb1, Yef3, Cam1, Dhh1, and eIF5A) and chaperones (Ssz1, Zuo1, and Ssb1) was downregulated (Figure 1C; Table S1). The expression levels of the components of degradation machineries were also changed. For example, the Dcp2 subunit of the decapping complex was upregulated in *not5Δ* (Figure 1C), but Pat1, a translational repressor (Marnef and Standart, 2010) and a deadenylation-decapping factor, reported to interact with Not5 to activate decapping (Alhusaini and Coller, 2016), was downregulated. Similarly, the 5′-to-3′ exonuclease Xrn1 was downregulated and accumulated in aggregates (Table S1). In *not4Δ*, the synthesis of these proteins was both up- and downregulated even though RPF levels were slightly downregulated. The exception was eIF5A whose new production and mRNA RPF levels were downregulated in both *not4Δ* and *not5Δ*.

In contrast, translation of the 3′-to-5′ exosome was enhanced slightly in *not4Δ* and significantly in *not5Δ* (Figures 1C and 1D). An increase in the expression of exosome mRNAs was previously described in cells lacking Not2 (Azzouz et al., 2009b), which is the heterodimeric partner of Not5 (Azzouz et al.,

CellPress
OPEN ACCESS

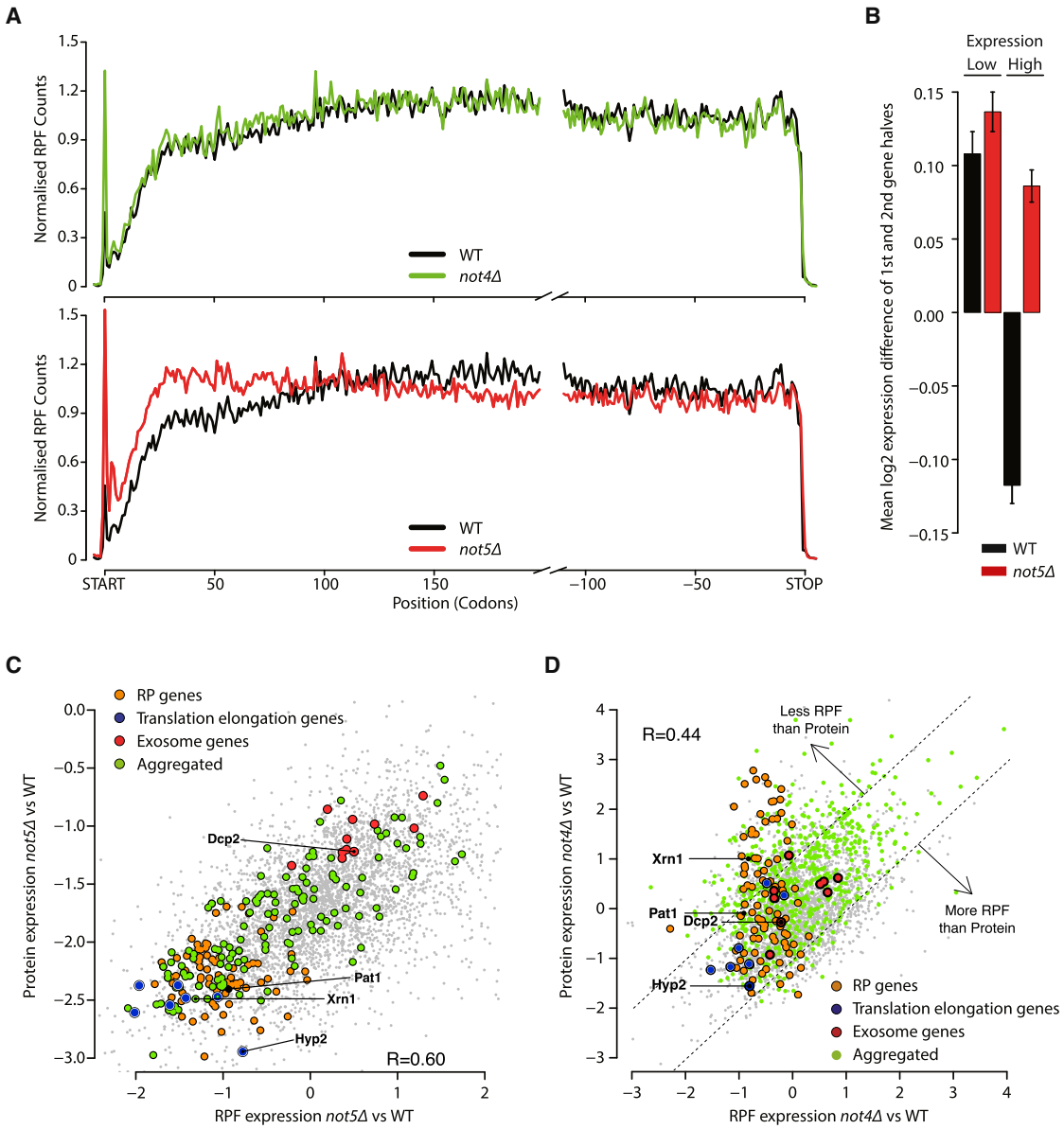

Figure 1. Translation elongation is altered in *not5Δ* and changes in the production of new proteins and RPFs in *not4Δ* and *not5Δ* versus the wild-type correlate

(A) Metagene analysis in wild type, *not4Δ* (top), and *not5Δ* (bottom).

(B) Mean RPKM ratio of both halves of open reading frames (ORFs) in *not5Δ* and wild type, split by high and low expression (greater or lesser than median expression, n = 2,524 in each group). SEM (standard error of the mean) is represented as error bars. A t test was used to compare wild type and *not5Δ* for $\log_2$ expression difference of 1st and 2nd gene halves; low expression genes, p = 0.1572979; high expression genes, p = 1.213031e-34.

(C) Comparison of normalized RPF (RiboSeq) and protein expression (SILAC [Gupta et al., 2016]) changes in *not5Δ* versus wild type. R, Pearson correlation coefficient. Specific proteins are indicated (Hyp2 is eIF5A).

(D) Comparison as in (C) for *not4Δ* versus wild type. Lines indicate cutoffs for significant differences in changes in the production of new proteins relative to changes in RPFs in *not4Δ* versus wild type. See also Tables S1 and S2.

2009a). This increase may occur to compensate for the defective deadenylation in *not5Δ*. However, the overall increased expression of the exosome in *not5Δ* may not necessarily correlate with increased activity because the integrity of the exosome might be compromised in *not5Δ*, as already described for other multi-subunit protein complexes, such as RNA polymerase II (Villanyi et al., 2014), the SAGA complex (Kassem et al., 2017), and the proteasome (Panasenko and Collart, 2011; Panasenko et al., 2019).

Taken together, these results indicate that changes in *de novo* protein production correlate well with changes in RPFs in cells lacking Not5 and to a lesser extent with Not4 deletion. Translation

is generally reduced in cells lacking Not5, with significant downregulation of the components of the translation apparatus. However, in *not4Δ*, the overall translation levels were similar to those in WT cells, and new RPs and translation elongation factors appear effectively synthesized despite mRNAs displaying reduced RPFs.

Transcripts with increased translation have increased RPFs at the start in *not4Δ* and *not5Δ*

We next focused on the accumulation of RPFs at the CDS start in both *not4Δ* and *not5Δ*. In principle, such an accumulation suggests defective initiation. Strikingly, the mRNA sets differ, whereby 297 were unique for *not4Δ* and 563 for *not5Δ* and 524 mRNAs were shared between both *not4Δ* and *not5Δ* (Figure S2A). These mRNAs also exhibit different functions (Table S2), as follows: in *not4Δ*, mostly mRNAs participating in protein complex biogenesis were enriched; in *not5Δ*, mRNAs with function in RNA binding, chromatin binding, mitochondrial translation, and proteolysis were enriched, and the shared set consisted of mRNAs encoding components of the vacuole, cell wall, and protein folding. These are all functions for which the relevance of the Ccr4-Not complex has been previously shown (Collart, 2016).

The metagene profiles of mRNAs divided as to whether they had increased footprints at start were similar for all three mRNA sets in WT and mutants (compare Figure S2B with Figure 1A). Comparing transcripts with peaks at start (high RPFs relative to the downstream region) in either *not4Δ* or *not5Δ* or both to a background of all genes, we observed a significant increase in RPFs relative to WT over the whole CDS in *not4Δ* and *not5Δ* (Figure S2C). Groups with peaks in *not4Δ* or *not5Δ* also showed significant increases in protein production in *not4Δ* or *not5Δ*, respectively (Figure S2D). Thus, mRNAs with peaks at start in *not4Δ* and *not5Δ* exhibited more upregulated translation in *not4Δ* and *not5Δ* than mRNAs overall.

Not5 affects translation elongation dynamics according to codon optimality

Translation elongation dynamics is important for co-translational events such as protein folding (Zhang and Ignatova, 2011). The massive aggregation of newly synthesized proteins in cells lacking Not4 and Not5 suggests an alteration of translation elongation dynamics. To mechanistically address this suggestion, first in *not5Δ*, we determined the ribosome dwelling occupancy (RDO) at each codon in the ribosomal A and P sites by calibrating the 5′ ends of RPFs to the start codon (Woolstenhulme et al., 2015). Because codons with high A-site RDOs are decoded by low-abundance tRNAs and thus are elongated at slower speed and, vice versa, codons decoded by high-abundance tRNAs exhibit lower RDO, we defined the differential or relative RDO of a codon as the $\log_2$- fold change (FC) of its RDO in *not5Δ* over WT and compared it to the tRNA adaptation index (tAI, calculated in Pechmann and Frydman, 2013). We defined as optimal codons the 15 codons with the highest tAI and as non-optimal the 15 codons with the lowest tAI. Compared with the WT strain, the A-site RDOs in *not5Δ* were markedly altered. Among the codons with lower RDOs, i.e., fast translated optimal codons, the RDOs were further decreased in *not5*Δ (proportion test; $p = 0.01127$; $\log_2FC < -0.2$) relative to the codons with higher RDO ($\log_2FC > 0.2$), whereas at the most non-optimal codons, the RDOs further increased in the mutant ($p = 0.04327$) (Figure 2A). Consistently, there was an overall inverse correlation between these changes in RDOs and tAI (Figure 2B).

RDO changes in *not5Δ* are robust and unrelated to mRNA codon composition and turnover

We next asked whether specific parameters might correlate with the observed codon-specific changes in A-site RDOs in *not5Δ*. We noted that they were the same for transcripts with low or high expression (Figure S3A), despite the overall anti-correlated codon frequencies between these two groups, with non-optimal codons being relatively more prevalent in the low expression group and optimal codons found more often in the high expression group (Figure S3B). We also noticed that the proportion of codons with increased or decreased RDOs in *not5Δ* compared to WT significantly differed between the first 75 codons of the 5′ CDS ends, where we also observed a marked RPF increase in *not5Δ*, to a downstream segment at 125–200 codons, where we observed a loss (Figure S3C). However, the percentage of non-optimal codons differed only by 1% between the first 100 codons of the CDS and the downstream region. Hence, the codon optimality alone is unlikely to directly account for the alteration of the metagene profile in *not5Δ*. Equally, the changes in A-site RDOs are unlikely to result from increased RPF counts in *not5Δ* at the 5′ end of transcripts because, as mentioned above, their distribution is well preserved between transcripts with low and high overall RPFs (Figure S3A); although, the high expression group shows significantly greater increases in the 5′ region in *not5Δ* (Figure 1B).

Because mRNA turnover can influence the overall RPF distribution, we checked whether A-site RDO changes in *not5Δ* might be connected to changes in mRNA turnover. We first focused on codons with increased A-site RDOs and considered the possibility that they could result from defective mRNA turnover. In such a model, one would expect increases in A-site RDOs at non-optimal codons to be greater for mRNAs containing more non-optimal codons, as their effect on mRNA stabilization would be cumulative. We extracted mRNAs scoring in the quartile with the most non-optimal codons and compared the RDO changes in *not5Δ* versus WT and related them to the mRNAs in the quartile with the least non-optimal codons. We detected no difference (Figure S3D). In addition, RDOs did not differ for mRNAs up- or downregulated in cells lacking Not5 (Figure S3E). Hence, the RDO changes are not an indirect consequence of changes in the mRNA turnover. Inversely, we asked whether mRNAs bearing more codons with increased A-site RDOs in *not5Δ* would be upregulated in *not5Δ*. Again, there was no correlation in changes of mRNA expression according to the relative amount of such codons in *not5Δ* versus the WT. Some of the mRNAs with the highest content of such codons were even downregulated in the mutant. These mRNAs were also up- or downregulated in cells lacking Not4. Notably, there was an overall good correlation between Ccr4-dependent mRNA stability (Sun et al., 2013) and mRNAs with upregulated RPF levels in *not4Δ* and *not5Δ* (Figure S3F).

Transcripts with a high proportion of optimal codons with decreased A-site RDOs in *not5Δ* exhibited lower RPF counts in

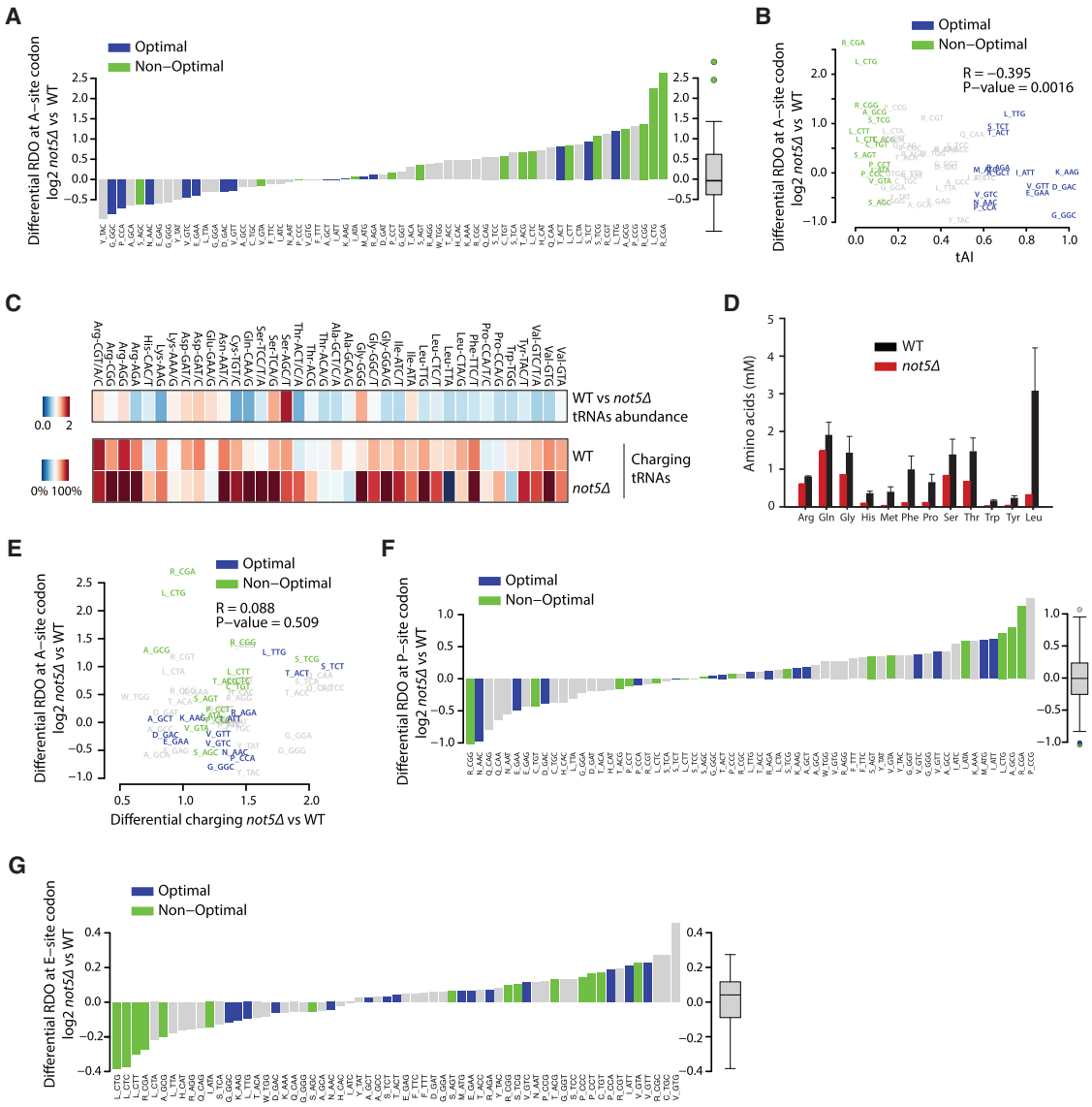

Figure 2. RDO changes in cells lacking Not5 are related to codon optimality but are not the consequence of charged tRNA levels

(A) RDO changes at A site codons in *not5Δ* relative to wild type, with 15 most-used (blue) and 15 least-used (green) codons. Gray, all other codons. Optimal codons are enriched in the lower RDO group in *not5Δ* (on the right: proportion test; p = 0.01127; $\log_2$FC < −0.2) relative to higher ($\log_2$FC > 0.2), and non-optimal codons are enriched in the higher RDO group (p = 0.04327).

(B) Scatterplot of tRNA adaptation index (tAI) versus the differential A-site RDO in *not5Δ* versus wild type.

(C) Microarray of total (abundance) and aminoacyl-tRNAs (charging) for two independent biological replicates. tRNA probes are depicted with their cognate codon and the corresponding amino acid. Total tRNA of *not5Δ* and wild type were hybridized, and the amount of each tRNA is directly comparable from the array. In the charging arrays, aminoacyl-tRNAs of each strain are hybridized along with total tRNAs and represented as % charged fraction for each tRNA.

(D) Metabolomic analysis of intracellular free amino acids. Error bars represent the standard deviation.

(E) Relative aminoacyl-tRNA charging levels (*not5Δ* versus wild type) for each cognate codon plotted against the relative A-site RDO ($\log_2$FC *not5Δ* versus wild type) of these codons. Charging FC was significantly increased in the higher RDO group (one-sided t test, p = 0.006229; $\log_2$FC > 0.2) relative to lower ($\log_2$FC < −0.2).

(F and G) Same as in (A) but for RDO changes at P site (F) and E site (G) codons. See also Tables S1 and S3.

not5Δ, as shown in particular for the highly expressed RP transcripts (Figure S3G). These mRNAs also contributed majorly to the reduced RPFs at the 3′ end of the ORFs in *not5Δ*, as shown for the RP mRNAs (Figure S3H), although this is clearly detectable even after excluding the RP transcripts from the analysis (Figure S3I). This reduction of RPFs at the 3′ end of highly expressed mRNAs could result from mRNA decay affecting specifically the 3′ end of mRNAs. However, in previous work, we measured total RP mRNA levels by using oligonucleotides pairing to the 3′ ends of the mRNA and found that they were either

unchanged or even elevated in *not5Δ* compared to the WT (Gupta et al., 2016). It thus seems unlikely that the decreased RPFs at the 3′ end of RP transcripts resulted from increased degradation of RP mRNA 3′ ends.

Taken together, these results indicate that RDO changes are very robust in *not5Δ* and are not related to mRNA context, the overall codon content, or changes in the expression or turnover of the mRNA.

Codon-specific A-site RDO changes are not due to changes in charged tRNA levels

The concentration of the cognate aminoacyl-tRNA is one major determinant of the ribosome speed at a codon in the ribosomal A site. Hence, we reasoned that the A-site RDOs might correlate with the concentration of the cognate aminoacyl-tRNAs. We measured the concentrations of total and aminoacylated tRNAs by using tRNA-tailored microarrays. The overall expression of tRNAs was similar between *not5Δ* and WT with the exception of a few upregulated tRNAs (e.g., tRNAs reading Ser-AGC/T, Ser-TCA/G, and Gly-GGG codons) and downregulated tRNAs (e.g., tRNAs reading Lys-AAG, Gln-CAA/G, Cys-TGC/T, and Thr-ACT/C/A codons) (Figure 2C, top; Table S3). These changes, albeit detectable, were marginal and slightly over the measuring noise. Clearly, the altered A-site RDOs in *not5Δ* did not correspond to cognate tRNA paucity or to cognate aminoacyl-tRNA paucity. On the contrary, aminoacyl-tRNA levels generally increased in *not5Δ*, which corresponded to the overall lower concentration of free amino acids in *not5Δ* (Figure 2D).

We considered whether the shortage of amino acids in *not5Δ*, despite growing in rich medium usually unlimited in amino acids, could explain the lower charging and slow translation of specific codons. For the majority of the measured free amino acids, we saw a clear decrease in their amount, and yet their cognate tRNAs were even more charged in *not5Δ* (e.g., $tRNAs^{Arg}$, $tRNAs^{Gly}$, $tRNA^{His}$, $tRNA^{Phe}$, $tRNAs^{Pro}$, $tRNAs^{Ser}$, $tRNAs^{Thr}$, $tRNA^{Trp}$, $tRNA^{Tyr}$, and two out of four $tRNAs^{Leu}$; Figure 2A), arguing against amino acid limitations, and consequently decreased aminoacyl-tRNAs altering RDOs at cognate codons (Figure 2D). The level of leucine, which is nonessential in budding yeast, was the most severely decreased in *not5Δ*. However, two out of four $tRNA^{Leu}$ isoacceptors were charged at a higher extent in *not5Δ* than in the WT strain. Notably, both $tRNAs^{Leu}$ decoding rare and high-abundance codons were highly charged, which cumulatively argues against the concentration of free leucine being limiting for charging. The cytosolic concentration of free amino acids did not directly reflect the charging of the tRNAs. This finding is supported by the fact that not only low-abundance tRNAs were more charged in *not5Δ* but also high-abundance tRNAs (i.e., those include the tRNA reading UUA that is the Leu codon with highest abundance). Importantly, changes in the A-site RDOs did not correlate with the aminoacyl-tRNA abundance (Figure 2E). Instead, the global accumulation of charged tRNAs that are not used in translation is consistent with an overall reduction of translation elongation, as seen also for other organisms (Tameire et al., 2019), which is in line with the above suggested global Not5-dependent elongation defect.

The RDO changes at the P site in *not5Δ* were less prominent than those at the A site, without any correlation to codon use (Figure 2F). Notably, among the five codons with the highest RDOs in *not5Δ*, four of them were similar in both the A and P site, e.g., Arg-CGA, Leu-CTG, Pro-CCG, and Ala-GCG (Figures 2A and 2F). Because Not5 was reported to bind the ribosomal E site (Buschauer et al., 2020), we also analyzed the RDO changes at the ribosomal E site in *not5Δ* versus control strain (Figure 2G). In contrast to the RDOs increased for the majority of Leu codons when in the A site (Figure 2A), for the E site, the RDO for all Leu codons was decreased in *not5Δ* relative to the WT, with three showing the highest RDO decrease, i.e., with the fastest dwelling at the E site.

Not4 and Not5 collaborate with Not1 to directly modulate translation elongation dynamics

We next addressed the mechanistic details of translation elongation changes in *not4Δ*. In this mutant, we observed codon-specific alterations in the RPF coverage (Figure 3A) that do not correspond to changes in the tRNA levels (Figure S4A) or free amino acid levels (Figure S4B), and they were unrelated to codon optimality. Curiously, A-site RDO changes in *not4Δ* showed only very weak correlation to those in *not5Δ* (Figure 3B).

RiboSeq is a powerful method with which to evaluate ribosome dwelling, and yet it may underestimate features, such as ribosome splitting and drop off. It has been shown that 5′-to-3′ co-translational decay follows the last translating ribosome and shows 3 nucleotide periodicity (Pelechano et al., 2015). We thus decided to use 5′P-Seq as an alternative method to compare ribosome dwelling (5′P-RDO) in cells lacking Not4 or Not5. We compared codon-specific A-site RDO changes from the RiboSeq to those evaluated using mean relative 5′P-Seq depth, 17 nucleotides (nt) upstream of each codon type, in the mutants relative to those of the WT. A significant correlation was observed for *not5Δ* (Figure 3C) but not for *not4Δ* (Figure 3D). In turn, the correlation of 5′P-RDO changes in *not4Δ* and *not5Δ* was nearly perfect (Figure 3E). Plotting WT pausing against *not4Δ* and *not5Δ* pausing directly, we also see that the consistent deviations from WT in the two mutants are not a result of small changes. Both mutants show a clear skew away from WT among low-frequency, non-optimal codons (Figures S4C and S4D). This finding clearly provides evidence that Not4 and Not5 work together during translation for co-translational decay, with identical alterations of codon-specific 5′-to-3′ decay intermediates in the absence of Not4 or Not5, inversely correlating with codon optimality; the latter is also seen for the A-site RDO changes in *not5Δ* by RiboSeq (Figure 2B).

To understand why RDO and 5′P-RDO changes correlated for *not5Δ* but not for *not4Δ*, we used published RiboSeq and 5′P-Seq data obtained in strains upon depletion of eIF5A (Pelechano and Alepuz, 2017; Schuller et al., 2017). We noted the absence of correlation (Figure 3F). Hence, it was when Not5 was deleted that the ribosome dwelling changes defined by ribosome footprints (RDO) and by co-translational decay intermediates (5′P-RDO) correlated. This result suggests that the Not5 deletion made RPFs from the pool of mRNAs undergoing co-translational decay mostly detectable by RiboSeq.

Not4 and Not5 are connected in the Ccr4-Not complex by the Not1 scaffold. To investigate if Not4 and Not5 modulate A-site

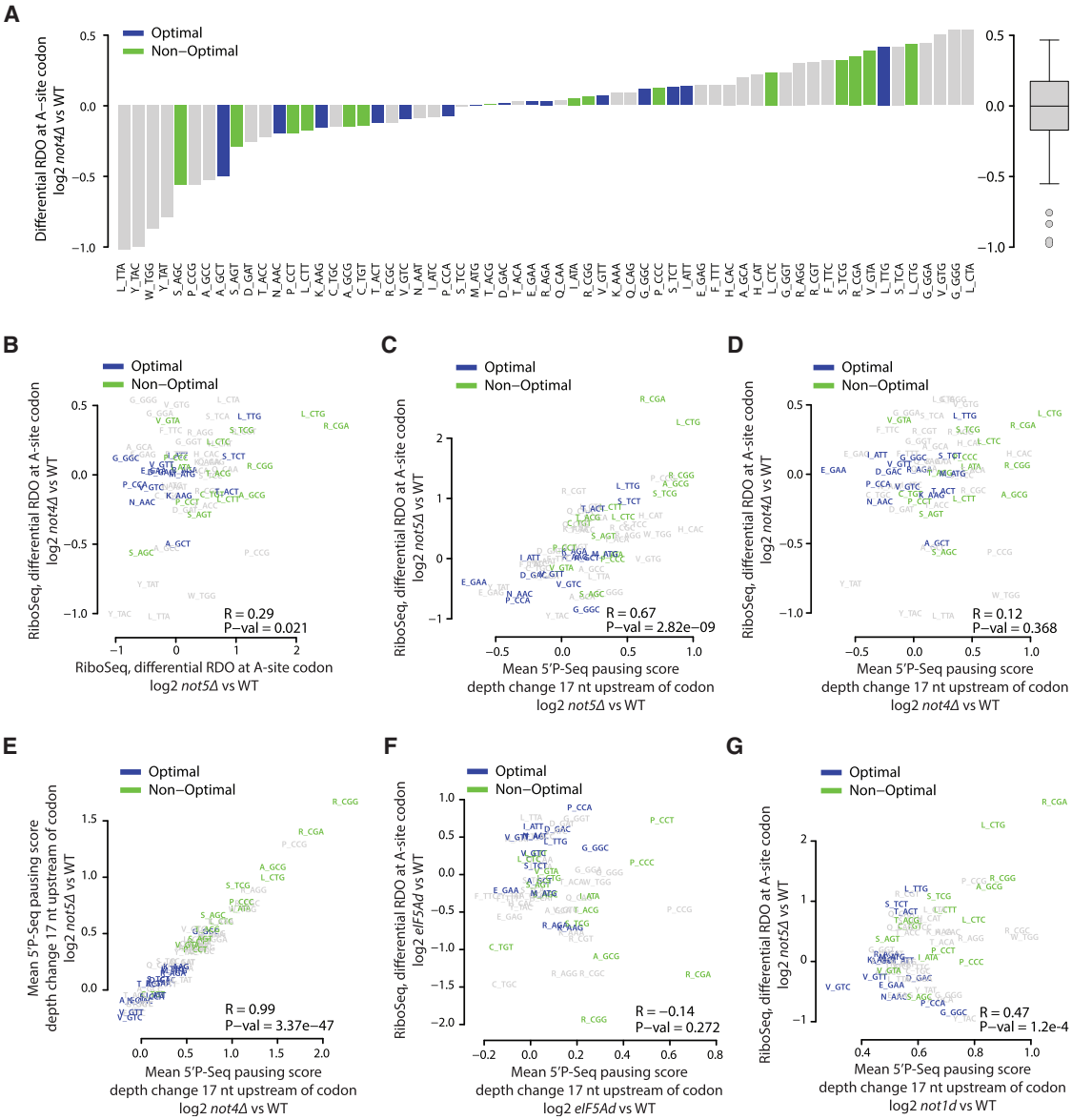

Figure 3. Not subunits of the Ccr4-Not complex collaborate to directly modulate translation elongation dynamics

(A) RDO changes at A site codons in *not4Δ* relative to wild type as in Figure 2A.

(B–G) Scatterplots of RDO changes at A site codons calculated from ribosome profiling (RiboSeq RDO changes, using mean relative A site depth in RPFs at each codon type) and 5′P-Seq depth changes (using mean relative 5′P-Seq depth, 17 nt upstream of each codon type). (B) RiboSeq RDO changes in *not4Δ* versus *not5Δ* relative to wild type. RiboSeq RDO changes versus 5′P-Seq depth changes in *not5Δ* relative to wild type (C) and in *not4Δ* relative to wild type (D). (E) 5′P-Seq depth changes in *not4Δ* versus *not5Δ* relative to wild type. (F) RiboSeq RDO changes versus 5′P-Seq depth changes for eIF5A depletion (*eIF5Ad*) over wild type. (G) RiboSeq RDO changes in *not5Δ* versus 5′P-Seq depth changes upon Not1 depletion (*not1d*). See also Table S1.

RDOs in the context of the Ccr4-Not complex, we created an auxin-inducible degron for Not1 (Figure S4E) and using 5′P-Seq evaluated changes in A-site RDOs following depletion of Not1. The A-site 5′P-RDO changes correlated with those in *not4Δ* or *not5Δ* (Figures S5A and S5B) and with RDO changes obtained by RiboSeq in *not5Δ* (Figure 3G). Taken together, these results support that Not4 and Not5, together with Not1, directly and collaboratively modulate translation elongation dynamics.

Interactions between Not4, Not5, and Rli1 regulate translation elongation

We imagined two possible scenarios to explain how Not5 might affect detectable RPFs of mRNAs undergoing co-translational decay. It could be that Not5 can tether translating mRNAs to condensates, removing them from lysates. Alternatively, Not5 might affect abortive translation and ribosome splitting, affecting the half-life of recoverable RPFs. The Rli1 ATPase is key for commonly splitting ribosomes at termination or during RQC

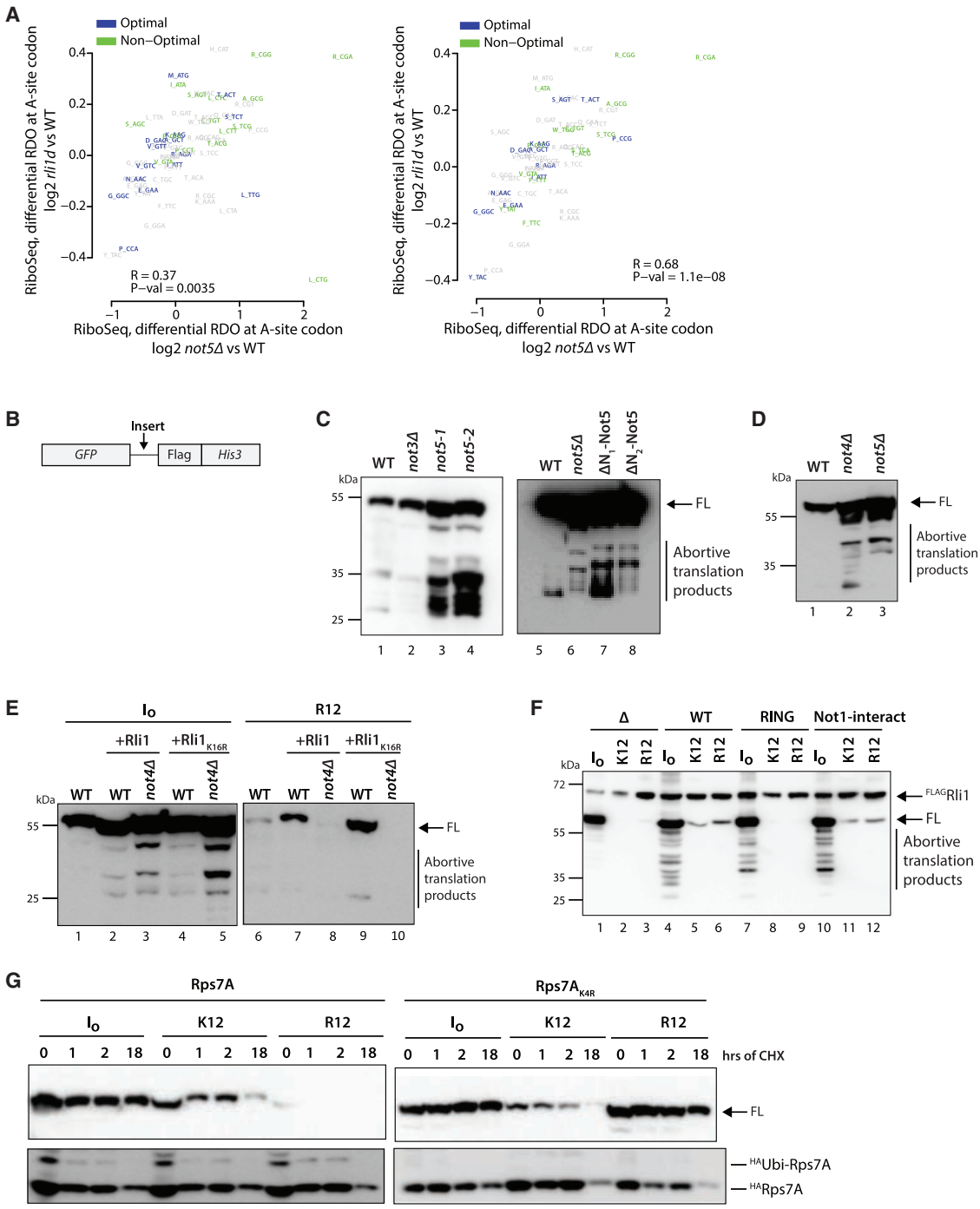

Figure 4. Not4 and Not5 both work both in concert and opposition to Rli1 moonlighting to regulate translation elongation

(A) Scatterplot of differential A-site RDOs for Rli1 depletion (*rli1d*) versus *not5Δ* over wild type with (left panel) or without (right panel) Leu codons.

(B) Cartoon of the reporter used in this figure, indicating the position where stalling sequences are inserted when mentioned.

(C–G) Expression of the reporter without (Io, C–G) or with (E–G) inserted stalling sequences, either 12 Lys codons (K12) or 12 Arg codons (R12), measured by western blotting with antibodies to FLAG. (C) *gcn4Δ* wild type, *not3Δ*, *not5-1*, and *not5-2* nonsense mutants (Oberholzer and Collart, 1998) (lanes 1–4) and BY4741 wild type, *not5Δ*, or *not5Δ* cells transformed with plasmids expressing N-terminally Myc6-tagged Not5 derivatives from amino acid 71 and 104, respectively (ΔN_1-Not5 and ΔN_2-Not5) (lanes 5–8). (D) BY4739 wild type, *not4Δ*, or *not5Δ*. (E) BY4741 wild type or wild type and *not4Δ* transformed with plasmids overexpressing wild-type Rli1 or $Rli1_{K16R}$. (F) W303 *not4Δ* transformed with a control plasmid (Δ), a plasmid expressing WT Not4 (WT), a RING mutant of Not4 (RING), or finally a Not1-interaction mutant of Not4 (Not1-interact). (G) W303-derived cells expressing hemagglutinin (HA)-tagged Rps7A or a non-ubiquitinated

(legend continued on next page)

(Young et al., 2015). It is the nexus between ribosome recycling and translation initiation (Mancera-Martínez et al., 2017). Recent work has indicated that it can be ubiquitinated by Not4 in flies (Wu et al., 2018). We also observed that it was ubiquitinated in yeast in a Not4-dependent manner (Figure S5C). We next used our pipeline to reanalyze RiboSeq data from the Rli1-depletion strain (Young et al., 2015). Interestingly, in the Rli1-depleted background, we detected a similar relation between codon optimality and A-site RDO changes, as observed in *not5Δ* (Figure 4A, left panel). Excluding the Leu codons, the correlation increased to 0.68 (Figure 4A, right panel), which is much higher than that between *not4Δ* and *not5Δ* (Figure 3B).

Together with Rli1, Dom34 is also important for ribosome recycling (Dever and Green, 2012; Guydosh and Green, 2014). Thus, we also reanalyzed previously published Dom34-deletion RiboSeq data (Guydosh and Green, 2014). We detected no correlation between A-site RDO changes upon Dom34 and Not5 deletion (Figures S5D and S5E).

Next, we focused more specifically on abortive translation, and we took advantage of a reporter expressing the GFP-FLAG-His3 fusion protein (Dimitrova et al., 2009). This reporter (Figure 4B) was expressed in *not5Δ* or in cells expressing Not5 derivatives lacking the C-terminal domain (Oberholzer and Collart, 1998), which is known to mediate the interaction with Not1 (Bhaskar et al., 2013), or N-terminally truncated Not5 variants lacking the domain of ribosome association (Buschauer et al., 2020). In all *not5* mutants, we detected, along with the full-length FLAG reporter protein, a ladder of truncated FLAG derivatives (Figure 4C). WT cells or another mutant of the Ccr4-Not complex, *not3Δ*, expressed fewer truncated forms (Figure 4C, lanes 1, 2, and 5). Abortive translation products were observed in *not4* or *not5* mutants regardless of the genetic background (Figure 4D).

Next, to explore the possible role of Rli1 in abortive translation upon deletion of Not proteins, we overexpressed Rli1 in WT cells. This induced abortive translation products (Figure 4E, compare lanes 1 and 2). In an attempt to create a non-ubiquitinated Rli1, we mutated 16 lysines to arginines ($Rli1_{K16R}$). This mutant Rli1 was equally well expressed as the WT Rli1 (Figure S5F) but failed to complement the deletion of Rli1 in a plasmid shuffle assay, probably due to mutations in functional domains of Rli1, such as the P loop of the first Walker A motif. Its overexpression, however, exhibited the same effect as that of the WT Rli1 and increased abortive translation products (Figure 4E, compare lanes 2 and 4 to lane 1). The amount of abortive translation products upon Rli1 overexpression increased further in *not4Δ* (Figure 4E, compare lanes 3 and 5 to lanes 2 and 4).

Because we observed that depletion of Rli1 or deletion of Not5 resulted in increased A-site RDOs at Arg codons (Figure 4A), we tested the effect of Rli1 overexpression with a reporter inserting between GFP and FLAG a stretch of 12 Arg codons (R12) that stalls ribosomes (Dimitrova et al., 2009). WT cells expressed low amounts of such a full-length protein (Figure 4E, compare lane 6 to lane 1), which was however increased by overexpression of WT or mutant Rli1 (Figure 4E, lanes 7 and 9). This phenotype was the opposite to what has been observed previously in *not4Δ* and *not5Δ* (Dimitrova et al., 2009; Halter et al., 2014) but required Not4 (Figure 4E, lanes 8 and 10). We confirmed this phenotype in a different genetic background, which was complemented by WT Not4 or a C-terminally truncated Not4 that lacks its Not1-interaction domain but not by a RING deletion mutant of Not4 (Figure 4F). Using a different stalling sequence composed of 12 Lys codons (K12; Dimitrova et al., 2009), we observed the same effect (Figure 4F, compare lanes 5 and 11 to lanes 2 and 8). A known substrate of the Not4 E3 ligase is Rps7A (Panasenko and Collart, 2012), whose ubiquitination is important for non-canonical RQC (Ikeuchi et al., 2019) and Not5 retention in polysomes (Buschauer et al., 2020). Although the ubiquitination of Rps7A did not affect the expression of the reporter without the stalling sequence (Io), it significantly affected the R12 sequence translation, but not the K12 reporter expression (K12) (Figure 4G). These results indicate complex interactions between Not4, Not5, and Rli1 that affect translation (see the cartoon in Figure S5G).

Not5 affects mRNA partitioning in insoluble condensates from which eIF5A is excluded

As mentioned above, an alternative mechanism to explain how Not5 affects detectable RPFs could be that Not5 removes translating ribosomes from the soluble pool of mRNAs in a codon-specific manner. We recently described the existence of Not1 condensates that regulate the co-translational assembly of specific proteasome subunits (Panasenko et al., 2019). Not4 and Not5, like Not1, showed a punctated cytoplasmic localization (Figure 5A). Structural data suggest that the binding of Not5 and eIF5A to translating ribosomes is mutually exclusive (Buschauer et al., 2020). However, in yeast, eIF5A is more than 10-fold more abundant that Not5 (Ho et al., 2018), and considering this, it seems unlikely that Not5 could effectively compete with eIF5A for ribosome association. Yet, the inverse correlation we observed between the RDO changes at optimal and non-optimal codons upon eIF5A depletion and Not5 deletion (Figure 5B) ($R = -0.53$) suggests a competition between the two proteins. Contrary to the situation in *not5Δ*, optimal codons were significantly enriched among the codons with increased RDOs in the eIF5A-depleted dataset ($p = 0.016$ when compared in a proportion test to optimal codon frequency in the lower relative RDO group). The anti-correlation between *not5Δ* and *eIF5Ad* was much weaker when considering the mean relative RDOs at the amino acid level (Figures S6A and S6B) ($R = -0.21$). The variation of the relative RDOs among different codons coding for the same amino acid was lower in the eIF5A-depleted strain than in *not5Δ*. Consistently, eIF5A does not co-purify with Not5 (Table S4) even in cells overexpressing eIF5A (Figure 5C). This finding led us consider a model in which during translational elongation Not5-regulated mRNAs might be in Not condensates that in turn might exclude eIF5A. In support of this model is the lack of detectable eIF5A in Not5 condensates (Figures 5D and S6C).

derivative ($Rps7A_{K4R}$) to complement the deletion of endogenous *RPS7A* and *RPS7B*, at the indicated times (in h) after addition of cycloheximide (CHX). Revelation with antibodies to FLAG (top panels) and HA (bottom panels). Full-length (FL) and abortive translation products are indicated on the right. Western blots are representative of at least 3 biological replicates. See also Table S1.

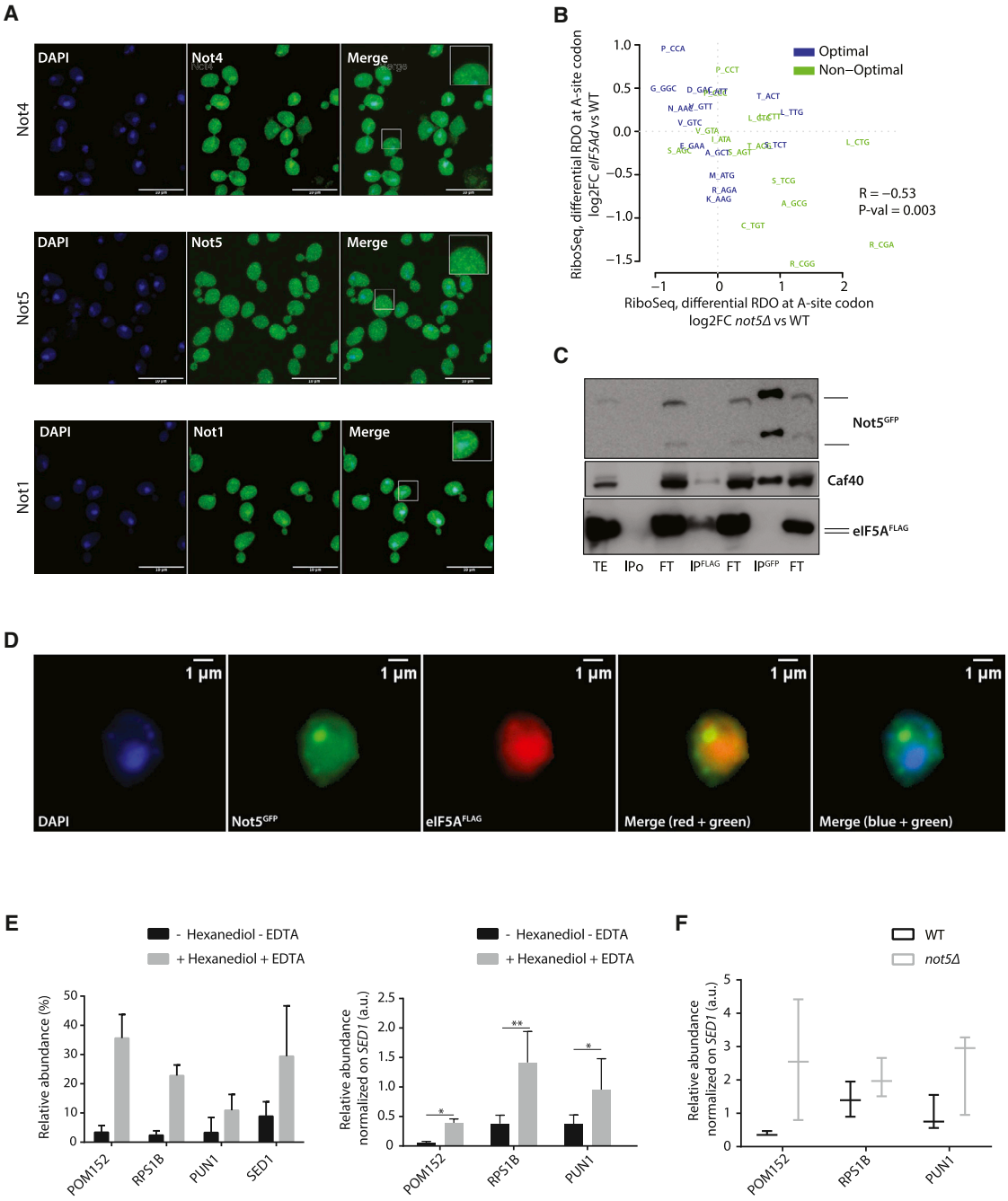

Figure 5. Not5 enhances partitioning of mRNAs into insoluble condensates

(A) Not4-GFP, Not5-GFP, and Not1-GFP localization in wild type, counterstained with DAPI (left panel), and the images were merged (right panel). Cells were imaged by confocal microscopy. Scale bar, 10 μm.

(B) Scatterplot of differential A-site RDOs for eIF5A depletion (*eIF5Ad*) over WT versus *not5Δ* over WT for 15 most-used (blue) and 15 least-used (green) codons.

(C) Extracts from cells expressing Not5-GFP from its endogenous locus and eIF5A-FLAG from a plasmid were incubated either without antibody (IPo) or with either antibodies to GFP (IP^{GFP}) or FLAG (IP^{FLAG}). Total and immunoprecipitated proteins were analyzed by western blotting with antibodies to FLAG, GFP, or Caf40. The presented result is representative of 2 biological replicates.

(D) Not5-GFP (green) and FLAG-eIF5A (red) localization in wild type counterstained with DAPI (blue, left panel), and the images were merged (last 2 right panels). Scale bar, 1 μm. This is a representative cell of n > 100. Additional cells are shown in Figure S6C.

(E) Levels of *SED1*, *PUN1*, *POM152*, and *RPS1B* transcripts measured in total RNA extracted with acid phenol or in the soluble RNA prepared by cell lysis as for polysome profiling with or without adding 1,6-hexanediol (200 mM) and EDTA (25 mM) in the lysis buffer. mRNA levels were expressed without (left panel) or with (right panel) normalization to *SED1* and presented as relative levels in soluble RNA pool versus total RNA pool (relative abundance) in arbitrary units (a.u.s). *PUN1*

(legend continued on next page)

From earlier work (Panasenko et al., 2019), we know that Not condensates with stalled ribosome-associated nascent chains (RNCs) can be partially solubilized from total cell extracts with RNaseA, increasing the levels of nascent chains from cell extracts sedimenting in heavy fractions of sucrose gradients despite the absence of polysomes. After RNaseA treatment of extracts prepared from cells expressing the Rpt1-RNC (Panasenko et al., 2019), Not1 and Not5 co-purified with the nascent chains isolated from the heavy fractions of a sucrose gradient, but no detectable eIF5A was found (Table S5). We next determined whether mRNAs partition to condensates, even in cells growing under optimal conditions, when no discernible stress granules are formed. We compared the levels of individual mRNAs in total extracts of cells lysed by hot-acid-phenol to those in soluble extracts (e.g., used for polysome profiling), which were prepared without or with additional 1,6-hexanediol that dissolves phase-separated condensates such as stress granules (Wheeler et al., 2016) and EDTA that splits ribosomes. Less than 10% of all tested mRNAs were recovered in the soluble extracts, but they were more abundant in the 1,6-hexanediol- and EDTA-treated soluble extracts (Figure 5E). Even in 1,6-hexanediol- and EDTA-treated soluble extracts, we detected less than 50% of the tested mRNAs. However, their amount was higher in these treated soluble extracts in *not5Δ* ($p = 0.0451$ compared to WT) (Figure 5F). Hence, Not5 affects the partitioning of mRNAs out of solution.

Finally, as Not5-GFP displays punctate staining due to condensation in the cytoplasm, we were able to photobleach and follow the recovery of several condensates at the same time. The Not5 condensates were indeed dynamic (Figures 6A and S6D; Video S1).

DISCUSSION

In this work, we determined that Not4 and Not5, which are important for the production of a soluble proteome, regulate translation elongation dynamics in a coordinated manner with Not1. Our model that during elongation Not5 may affect the ribosome's fate through E-site binding, either at initiation or for ribosomes with a vacant A site at a non-optimal codon, is consistent with recent structural work (Buschauer et al., 2020). It is less clear how Not5 could affect ribosome dwelling at optimal codons where Not5 is unlikely to bind the ribosome. However, changes at optimal codons could be related to the ability of eIF5A to bind the ribosome, rather than Not5. Indeed, our data suggest effective competition between Not5 and eIF5A, which is in line with structural considerations (Buschauer et al., 2020).

We propose a model whereby Not5-driven condensates can pull RNCs out of solution and thereby exclude eIF5A from accessing the RNCs, enabling effective competition between Not5 and the more abundant eIF5A (Figure 6B). The hyperfluorescent Not5 foci in the cytosol are reminiscent of Not1-containing RNA condensates (assemblysomes [Panasenko et al., 2019]), which are active in translation. The Not5 condensates are dynamic according to their exchange rate after photobleaching. They are more dynamic than, for instance, most p-body components (Xing et al., 2020); however, they show similarity to the dynamics of Not2 and Ccr4 in the p-bodies. Furthermore, other dynamic properties of the Not5 condensates (e.g., low mobile fraction and half-time recovery) are reminiscent of those observed for Pub1 condensates upon heat-stress adaptation (Kroschwald et al., 2018). According to our model, a decondensation renders the RNCs accessible to eIF5A. If decondensation occurs with a non-optimal codon in the A site, Not5 might be bound, allowing a new cycle of condensation. This mechanism is compatible with slower translation elongation at the beginning of mRNAs enriched with non-optimal codons. The effect of Not5 deletion at optimal codons, such as the proline CCA codon, could result from a better overall access of eIF5A to RNCs in the absence of Not5 condensation.

In our work, we also determined that depletion of Rli1 and deletion of Not5 affect A-site RDO similarly, but in a Dom34-independent manner. According to our model (Figure 6B), Not5 affects RDOs by condensation, and hence, Rli1 might participate in this condensation mechanism. Curiously, overexpression of Rli1 increased abortive translation similarly to the deletion of Not4 or Not5. Previous work has shown that the overexpressed mutant Rli1 reduces the levels of polysomes relative to monosomes, likely as a result of reduced translation initiation (Dong et al., 2004). However, overexpressing WT Rli1 had a similar effect. Abortive translation upon Rli1 overexpression is compatible with these previous findings. We propose that abortive translation does not occur by the canonical ribosome splitting function of Rli1, which would need a functional Rli1, but rather through an alternative moonlighting function. Besides abortive translation, the Rli1 overexpression also enables translation of poly-Arg stretches in a cooperation with Not4, and in particular its RING domain. Rps7A is a target of Not4 ubiquitination, but preventing Rps7A ubiquitination had the same phenotype as Rli1 overexpression. This result indicates that Not4-dependent ubiquitination may serve to both promote and prevent translation of poly-Arg stretches. Consistent with this complex function of Not4, mutation of its RING domain inhibits translation of poly-Arg stretches, although it prevents Rps7A ubiquitination. In this context, it is interesting to note that Rli1 itself is a target of Not4 ubiquitination.

Rli1 is present at early initiation steps, whereas the Not proteins bind late initiation ribosomes. It is, thus, tempting to speculate that together they can start condensation cycles at the very start of translation. Cycles of condensation and decondensation of Not5 are compatible with the observed dynamic nature of Not5 condensates. Competing with new cycles of condensation,

has the lowest optimal codon content among mRNAs upregulated in *not5Δ*, and *RPS1B* the highest among mRNAs downregulated in *not5Δ*. *POM152* is unchanged. *SED1* mRNA is not bound by Not1 (Gupta et al., 2016) and was chosen for normalization. Error bars represent the standard deviation.
(F) The levels of the same mRNAs relative to *SED1* in extracts with 1,6-hexanediol (200 mM) and EDTA (25 mM) in the lysis buffer compared to total RNA extracted with acid phenol were compared between wild type and *not5Δ*. A fixed effects model was fitted with relative abundance as a dependent variable and strain (wild type and *not5Δ*) as a fixed effect ($p = 0.0451$ for the fixed coefficient test). Transcripts and technical duplicates were encoded as random effects. $n = 3$ for RNA samples, and error bars are mean squared error. See also Tables S1, S4, and S5.

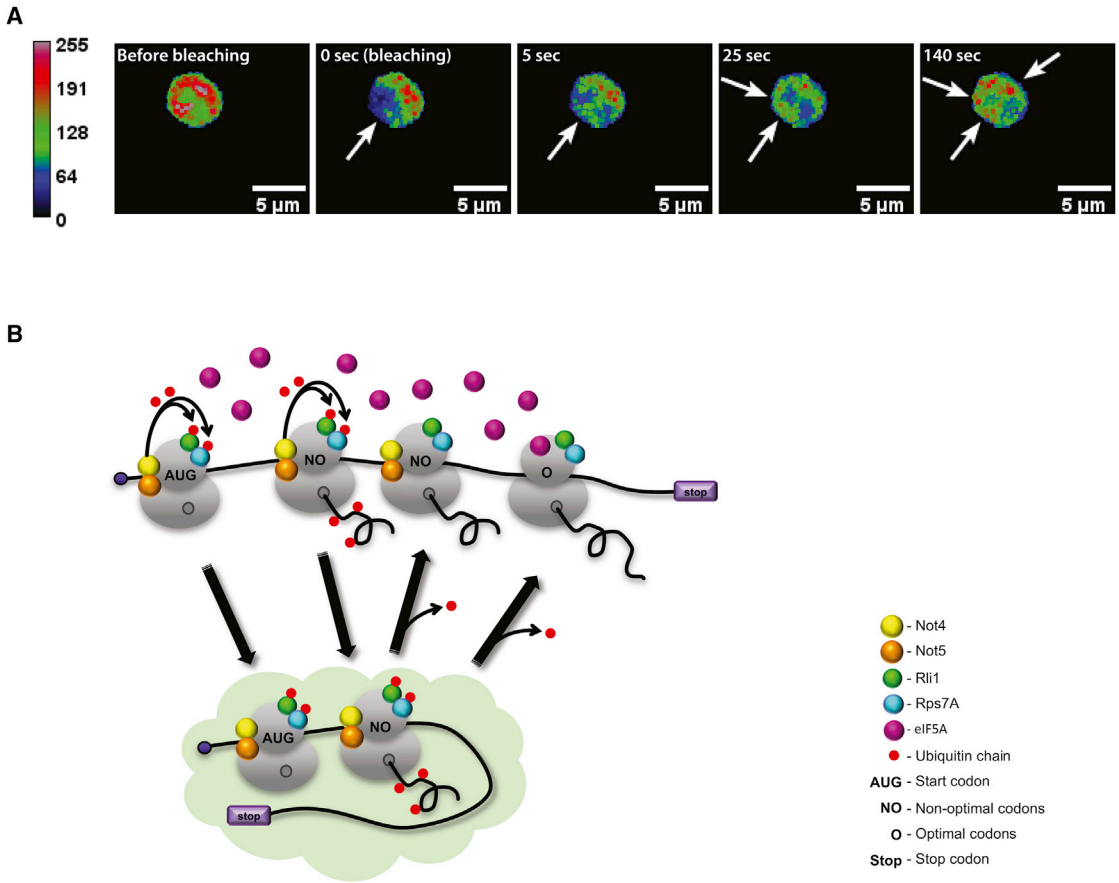

Figure 6. Not condensates enable effective competition between Not5 and eIF5A

(A) Wild-type cells expressing Not5-GFP were visualized prior to, and at different times after, bleaching. White arrows indicate sites where condensates can be visualized changing over time. Scale bar, 5 μm. The rainbow-colored images are artificially enhanced to highlight the punctate Not5-GFP-related fluorescence signals despite the small size of the condensates and the limit of the microscope magnification (see STAR Methods). The calibration bar shows the fluorescence values (red, high intensity; blue, low intensity).

(B) Model to explain how Not proteins regulate translation elongation dynamics. Upon Not5 ribosome binding together with Not4, mRNAs can partition into condensates, regulated by Not4, Rli1, and ubiquitination of Rps7A. This can occur first at start but reoccur when translating ribosomes are released from condensates with a non-optimal codon in the A site, and Not5 is associated at the E site. Cycles of ubiquitination and deubiquitination are likely to contribute to regulating condensation. Ribosomes released from condensates are accessible to eIF5A. In *not4Δ* and *not5Δ*, RPFs from mRNAs in condensates in wild-type cells increase in RiboSeq experiments, in particular ribosomes at start and at non-optimal codons. See also Tables S4 and S5.

ribosome-associated Not5 might alternatively recruit the decapping activator Pat1 or induce deadenylation and 5′-to-3′ decay by Xrn1, which is compatible with the reported 5′-to-3′ decay following the last translating ribosome (Pelechano et al., 2015), and explain the higher instability of mRNAs with a higher content of non-optimal codons. Alternatively, if RNCs do not condensate at non-optimal codons, eIF5A can access the RNCs and decrease ribosome dwelling at proline codons but may also raise the risk of ribosome collisions resulting in mRNA decay at downstream non-optimal codons.

Our model consistently framed all our experimental data, which were generated using strains that have been growing for generations after the deletion of genes important for WT growth. It is possible that such cells acquire compensatory mutations or display phenotypes that are indirect consequences of the altered growth. Moreover, all measurements were at steady state and any kinetic effects remained undetected. In the future, the use of our Not1 degron strain, and similar Not4 and Not5 degron strains, will be important for addressing this model more directly. An important question will be whether the increase of ribosomes at specific codons in mutants (i.e., paused ribosomes) correspond to those that are sequestered in the condensates.

STAR★METHODS

Detailed methods are provided in the online version of this paper and include the following:

- KEY RESOURCES TABLE
- RESOURCE AVAILABILITY
  - Lead contact
  - Materials availability
  - Data and code availability
- EXPERIMENTAL MODEL AND SUBJECT DETAILS

SUPPLEMENTAL INFORMATION

Supplemental information can be found online at https://doi.org/10.1016/j.celrep.2021.109633.

ACKNOWLEDGMENTS

We are grateful to Dr. Ulrike Rolle-Kampczyk and Dr. Martin von Bergen (Helmholz for Environmental Research, Leipzig, Germany) for the amino acid metabolomics measurements. This work was supported by grant 31003A_172999 from the Swiss National Science Foundation awarded to M.A.C.; grants GINOP-2.3.2-15-2016-00020 and ÚNKP-19-4-SZTE-118 from the Hungarian National Research, Development and Innovation Office and the János Bolyai Research Scholarship of the Hungarian Academy of Sciences awarded to Z.V.; a Helmut Horten Stiftung grant awarded to O.O.P.; grant FOR1805 (Deutsche Forschungsgemeinschaft) awarded to Z.I.; and the Ragnar Söderberg Foundation, Wallenberg Academy Fellowship (KAW 2016.0123) as well as the Swedish Research Council (VR 2016-01842) to V.P.

AUTHOR CONTRIBUTIONS

G.E.A. performed RiboSeq, 5′P-Seq, and SILAC analysis. O.O.P. performed RiboSeq. Z.V. prepared the samples for aggregate, tRNA, and metabolomic analyses. O.O.P. and Z.V. also contributed to the scientific design. M.Z. did reporter gene expression, coIP, FRAP, and immunofluorescence experiments. B.W. did RNA preparations, analyses, and manuscript figures. S.H. made the 5′P libraries and initial analyses with V.P.; C.P. performed and analyzed the tRNA microarrays; L.P. did immunofluorescence studies; S.Z. and Z.V. did the affinity purifications; S.Z. performed the FRAP analysis and figure preparations for the FRAP and immunofluorescence data; C.S.H. did the SILAC analysis; and Z.I. and M.A.C. analyzed data, supervised the work, and wrote the manuscript.

DECLARATION OF INTERESTS

There are no competing interests.

Received: October 5, 2020
Revised: March 18, 2021
Accepted: August 9, 2021
Published: August 31, 2021

REFERENCES

Albert, B., Kos-Braun, I.C., Henras, A.K., Dez, C., Rueda, M.P., Zhang, X., Gadal, O., Kos, M., and Shore, D. (2019). A ribosome assembly stress response regulates transcription to maintain proteome homeostasis. eLife *8*, e45002.

Alhusaini, N., and Coller, J. (2016). The deadenylase components Not2p, Not3p, and Not5p promote mRNA decapping. RNA *22*, 709–721.

Azzouz, N., Panasenko, O.O., Colau, G., and Collart, M.A. (2009a). The CCR4-NOT complex physically and functionally interacts with TRAMP and the nuclear exosome. PLoS One *4*, e6760.

Azzouz, N., Panasenko, O.O., Deluen, C., Hsieh, J., Theiler, G., and Collart, M.A. (2009b). Specific roles for the Ccr4-Not complex subunits in expression of the genome. RNA *15*, 377–383.

Benne, R., and Hershey, J.W. (1978). The mechanism of action of protein synthesis initiation factors from rabbit reticulocytes. J. Biol. Chem. *253*, 3078–3087.

Bhaskar, V., Roudko, V., Basquin, J., Sharma, K., Urlaub, H., Séraphin, B., and Conti, E. (2013). Structure and RNA-binding properties of the Not1-Not2-Not5 module of the yeast Ccr4-Not complex. Nat. Struct. Mol. Biol. *20*, 1281–1288.

Buschauer, R., Matsuo, Y., Sugiyama, T., Chen, Y.H., Alhusaini, N., Sweet, T., Ikeuchi, K., Cheng, J., Matsuki, Y., Nobuta, R., et al. (2020). The Ccr4-Not complex monitors the translating ribosome for codon optimality. Science *368*, eaay6912.

Collart, M.A. (2016). The Ccr4-Not complex is a key regulator of eukaryotic gene expression. Wiley Interdiscip Rev. RNA *7*, 438–454.

Collart, M.A., and Oliviero, S. (2001). Preparation of yeast RNA. Curr. Protoc. Mol. Biol. *Chapter 13*, Unit 13.12.

Collart, M.A., and Struhl, K. (1994). NOT1(CDC39), NOT2(CDC36), NOT3, and NOT4 encode a global-negative regulator of transcription that differentially affects TATA-element utilization. Genes Dev. *8*, 525–537.

Daugeron, M.C., Mauxion, F., and Séraphin, B. (2001). The yeast POP2 gene encodes a nuclease involved in mRNA deadenylation. Nucleic Acids Res. *29*, 2448–2455.

Dever, T.E., and Green, R. (2012). The elongation, termination, and recycling phases of translation in eukaryotes. Cold Spring Harb. Perspect. Biol. *4*, a013706.

Dietmair, S., Timmins, N.E., Gray, P.P., Nielsen, L.K., and Krömer, J.O. (2010). Towards quantitative metabolomics of mammalian cells: development of a metabolite extraction protocol. Anal. Biochem. *404*, 155–164.

Dimitrova, L.N., Kuroha, K., Tatematsu, T., and Inada, T. (2009). Nascent peptide-dependent translation arrest leads to Not4p-mediated protein degradation by the proteasome. J. Biol. Chem. *284*, 10343–10352.

Dong, J., Lai, R., Nielsen, K., Fekete, C.A., Qiu, H., and Hinnebusch, A.G. (2004). The essential ATP-binding cassette protein RLI1 functions in translation by promoting preinitiation complex assembly. J. Biol. Chem. *279*, 42157–42168.

Gupta, I., Villanyi, Z., Kassem, S., Hughes, C., Panasenko, O.O., Steinmetz, L.M., and Collart, M.A. (2016). Translational Capacity of a Cell Is Determined during Transcription Elongation via the Ccr4-Not Complex. Cell Rep. *15*, 1782–1794.

Guydosh, N.R., and Green, R. (2014). Dom34 rescues ribosomes in 3′ untranslated regions. Cell *156*, 950–962.

Halter, D., Collart, M.A., and Panasenko, O.O. (2014). The Not4 E3 ligase and CCR4 deadenylase play distinct roles in protein quality control. PLoS One *9*, e86218.

Ho, B., Baryshnikova, A., and Brown, G.W. (2018). Unification of Protein Abundance Datasets Yields a Quantitative Saccharomyces cerevisiae Proteome. Cell Syst. *6*, 192–205.e3.

Hope, I.A., and Struhl, K. (1986). Functional dissection of a eukaryotic transcriptional activator protein, GCN4 of yeast. Cell *46*, 885–894.

Hughes, C.S., Foehr, S., Garfield, D.A., Furlong, E.E., Steinmetz, L.M., and Krijgsveld, J. (2014). Ultrasensitive proteome analysis using paramagnetic bead technology. Mol. Syst. Biol. *10*, 757.

Hughes, C.S., McConechy, M.K., Cochrane, D.R., Nazeran, T., Karnezis, A.N., Huntsman, D.G., and Morin, G.B. (2016). Quantitative Profiling of Single Formalin Fixed Tumour Sections: proteomics for translational research. Sci. Rep. *6*, 34949.

Hughes, C.S., Moggridge, S., Müller, T., Sorensen, P.H., Morin, G.B., and Krijgsveld, J. (2019). Single-pot, solid-phase-enhanced sample preparation for proteomics experiments. Nat. Protoc. *14*, 68–85.

Ikeuchi, K., Tesina, P., Matsuo, Y., Sugiyama, T., Cheng, J., Saeki, Y., Tanaka, K., Becker, T., Beckmann, R., and Inada, T. (2019). Collided ribosomes form a unique structural interface to induce Hel2-driven quality control pathways. EMBO J. *38*, e100276.

Ingolia, N.T. (2016). Ribosome Footprint Profiling of Translation throughout the Genome. Cell *165*, 22–33.

Ingolia, N.T., Ghaemmaghami, S., Newman, J.R., and Weissman, J.S. (2009). Genome-wide analysis in vivo of translation with nucleotide resolution using ribosome profiling. Science *324*, 218–223.

Jansen, G., Wu, C., Schade, B., Thomas, D.Y., and Whiteway, M. (2005). Drag&Drop cloning in yeast. Gene *344*, 43–51.

Kassem, S., Villanyi, Z., and Collart, M.A. (2017). Not5-dependent co-translational assembly of Ada2 and Spt20 is essential for functional integrity of SAGA. Nucleic Acids Res. *45*, 1186–1199.

Kim, D., Langmead, B., and Salzberg, S.L. (2015). HISAT: a fast spliced aligner with low memory requirements. Nat. Methods *12*, 357–360.

Kirchner, S., Cai, Z., Rauscher, R., Kastelic, N., Anding, M., Czech, A., Kleizen, B., Ostedgaard, L.S., Braakman, I., Sheppard, D.N., and Ignatova, Z. (2017). Alteration of protein function by a silent polymorphism linked to tRNA abundance. PLoS Biol. *15*, e2000779.

Kroschwald, S., Munder, M.C., Maharana, S., Franzmann, T.M., Richter, D., Ruer, M., Hyman, A.A., and Alberti, S. (2018). Different Material States of Pub1 Condensates Define Distinct Modes of Stress Adaptation and Recovery. Cell Rep. *23*, 3327–3339.

Kruk, J.A., Dutta, A., Fu, J., Gilmour, D.S., and Reese, J.C. (2011). The multifunctional Ccr4-Not complex directly promotes transcription elongation. Genes Dev. *25*, 581–593.

Kuznetsova, A., Brockhoff, P., and Christensen, R. (2017). lmerTest Package: Tests in Linear Mixed Effects Models. J. Stat. Softw. *82*, 13.

Langmead, B., and Salzberg, S.L. (2012). Fast gapped-read alignment with Bowtie 2. Nat. Methods *9*, 357–359.

Lauria, F., Tebaldi, T., Bernabò, P., Groen, E.J.N., Gillingwater, T.H., and Viero, G. (2018). riboWaltz: Optimization of ribosome P-site positioning in ribosome profiling data. PLoS Comput. Biol. *14*, e1006169.

Li, H., Handsaker, B., Wysoker, A., Fennell, T., Ruan, J., Homer, N., Marth, G., Abecasis, G., and Durbin, R.; 1000 Genome Project Data Processing Subgroup (2009). The Sequence Alignment/Map format and SAMtools. Bioinformatics *25*, 2078–2079.

Longtine, M.S., McKenzie, A., III, Demarini, D.J., Shah, N.G., Wach, A., Brachat, A., Philippsen, P., and Pringle, J.R. (1998). Additional modules for versatile and economical PCR-based gene deletion and modification in *Saccharomyces cerevisiae*. Yeast *14*, 953–961.

Mancera-Martínez, E., Brito Querido, J., Valasek, L.S., Simonetti, A., and Hashem, Y. (2017). ABCE1: A special factor that orchestrates translation at the crossroad between recycling and initiation. RNA Biol. *14*, 1279–1285.

Marnef, A., and Standart, N. (2010). Pat1 proteins: a life in translation, translation repression and mRNA decay. Biochem. Soc. Trans. *38*, 1602–1607.

Martin, M. (2011). Cutadapt Removes Adapter Sequences from High-Throughput Sequencing Reads. EMBnet. J. *17*, 10–12.

Morawska, M., and Ulrich, H.D. (2013). An expanded tool kit for the auxin-inducible degron system in budding yeast. Yeast *30*, 341–351.

Oberholzer, U., and Collart, M.A. (1998). Characterization of NOT5 that encodes a new component of the Not protein complex. Gene *207*, 61–69.

Panasenko, O.O., and Collart, M.A. (2011). Not4 E3 ligase contributes to proteasome assembly and functional integrity in part through Ecm29. Mol. Cell. Biol. *31*, 1610–1623.

Panasenko, O.O., and Collart, M.A. (2012). Presence of Not5 and ubiquitinated Rps7A in polysome fractions depends upon the Not4 E3 ligase. Mol. Microbiol. *83*, 640–653.

Panasenko, O., Landrieux, E., Feuermann, M., Finka, A., Paquet, N., and Collart, M.A. (2006). The yeast Ccr4-Not complex controls ubiquitination of the nascent-associated polypeptide (NAC-EGD) complex. J. Biol. Chem. *281*, 31389–31398.

Panasenko, O.O., Somasekharan, S.P., Villanyi, Z., Zagatti, M., Bezrukov, F., Rashpa, R., Cornut, J., Iqbal, J., Longis, M., Carl, S.H., et al. (2019). Co-translational assembly of proteasome subunits in NOT1-containing assemblysomes. Nat. Struct. Mol. Biol. *26*, 110–120.

Pechmann, S., and Frydman, J. (2013). Evolutionary conservation of codon optimality reveals hidden signatures of cotranslational folding. Nat. Struct. Mol. Biol. *20*, 237–243.

Pelechano, V., and Alepuz, P. (2017). eIF5A facilitates translation termination globally and promotes the elongation of many non polyproline-specific tripeptide sequences. Nucleic Acids Res. *45*, 7326–7338.

Pelechano, V., Wei, W., and Steinmetz, L.M. (2015). Widespread Co-translational RNA Decay Reveals Ribosome Dynamics. Cell *161*, 1400–1412.

Preissler, S., Reuther, J., Koch, M., Scior, A., Bruderek, M., Frickey, T., and Deuerling, E. (2015). Not4-dependent translational repression is important for cellular protein homeostasis in yeast. EMBO J. *34*, 1905–1924.

Reese, J.C. (2013). The control of elongation by the yeast Ccr4-not complex. Biochim. Biophys. Acta *1829*, 127–133.

Reits, E.A., and Neefjes, J.J. (2001). From fixed to FRAP: measuring protein mobility and activity in living cells. Nat. Cell Biol. *3*, E145–E147.

Robinson, M.D., McCarthy, D.J., and Smyth, G.K. (2010). edgeR: a Bioconductor package for differential expression analysis of digital gene expression data. Bioinformatics *26*, 139–140.

Rouya, C., Siddiqui, N., Morita, M., Duchaine, T.F., Fabian, M.R., and Sonenberg, N. (2014). Human DDX6 effects miRNA-mediated gene silencing via direct binding to CNOT1. RNA *20*, 1398–1409.

Saini, P., Eyler, D.E., Green, R., and Dever, T.E. (2009). Hypusine-containing protein eIF5A promotes translation elongation. Nature *459*, 118–121.

Sandler, H., Kreth, J., Timmers, H.T., and Stoecklin, G. (2011). Not1 mediates recruitment of the deadenylase Caf1 to mRNAs targeted for degradation by tristetraprolin. Nucleic Acids Res. *39*, 4373–4386.

Schneider, C.A., Rasband, W.S., and Eliceiri, K.W. (2012). NIH Image to ImageJ: 25 years of image analysis. Nat. Methods *9*, 671–675.

Schuller, A.P., Wu, C.C., Dever, T.E., Buskirk, A.R., and Green, R. (2017). eIF5A Functions Globally in Translation Elongation and Termination. Mol. Cell *66*, 194–205.e5.

Stowell, J.A.W., Webster, M.W., Kögel, A., Wolf, J., Shelley, K.L., and Passmore, L.A. (2016). Reconstitution of Targeted Deadenylation by the Ccr4-Not Complex and the YTH Domain Protein Mmi1. Cell Rep. *17*, 1978–1989.

Sun, M., Schwalb, B., Pirkl, N., Maier, K.C., Schenk, A., Failmezger, H., Tresch, A., and Cramer, P. (2013). Global analysis of eukaryotic mRNA degradation reveals Xrn1-dependent buffering of transcript levels. Mol. Cell *52*, 52–62.

Tameire, F., Verginadis, I.I., Leli, N.M., Polte, C., Conn, C.S., Ojha, R., Salas Salinas, C., Chinga, F., Monroy, A.M., Fu, W., et al. (2019). ATF4 couples MYC-dependent translational activity to bioenergetic demands during tumour progression. Nat. Cell Biol. *21*, 889–899.

Tucker, M., Valencia-Sanchez, M.A., Staples, R.R., Chen, J., Denis, C.L., and Parker, R. (2001). The transcription factor associated Ccr4 and Caf1 proteins are components of the major cytoplasmic mRNA deadenylase in Saccharomyces cerevisiae. Cell *104*, 377–386.

Villanyi, Z., Ribaud, V., Kassem, S., Panasenko, O.O., Pahi, Z., Gupta, I., Steinmetz, L., Boros, I., and Collart, M.A. (2014). The Not5 subunit of the ccr4-not complex connects transcription and translation. PLoS Genet. *10*, e1004569.

Vizcaíno, J.A., Csordas, A., Del-Toro, N., Dianes, J.A., Griss, J., Lavidas, I., Mayer, G., Perez-Riverol, Y., Reisinger, F., Ternent, T., et al. (2016). 2016 update of the PRIDE database and its related tools. Nucleic Acids Res. *44*, 11033.

Wheeler, J.R., Matheny, T., Jain, S., Abrisch, R., and Parker, R. (2016). Distinct stages in stress granule assembly and disassembly. eLife *5*, e18413.

Wilcoxon, F. (1946). Individual comparisons of grouped data by ranking methods. J. Econ. Entomol. *39*, 269.

Willmund, F., del Alamo, M., Pechmann, S., Chen, T., Albanèse, V., Dammer, E.B., Peng, J., and Frydman, J. (2013). The cotranslational function of ribosome-associated Hsp70 in eukaryotic protein homeostasis. Cell *152*, 196–209.

Woolstenhulme, C.J., Guydosh, N.R., Green, R., and Buskirk, A.R. (2015). High-precision analysis of translational pausing by ribosome profiling in bacteria lacking EFP. Cell Rep. *11*, 13–21.

Wu, Z., Wang, Y., Lim, J., Liu, B., Li, Y., Vartak, R., Stankiewicz, T., Montgomery, S., and Lu, B. (2018). Ubiquitination of ABCE1 by NOT4 in Response to Mitochondrial Damage Links Co-translational Quality Control to PINK1-Directed Mitophagy. Cell Metab. *28*, 130–144.e7.

Xing, W., Muhlrad, D., Parker, R., and Rosen, M.K. (2020). A quantitative inventory of yeast P body proteins reveals principles of composition and specificity. eLife *9*, e56525.

Young, D.J., Guydosh, N.R., Zhang, F., Hinnebusch, A.G., and Green, R. (2015). Rli1/ABCE1 Recycles Terminating Ribosomes and Controls Translation Reinitiation in 3'UTRs In Vivo. Cell *162*, 872–884.

Zhang, G., and Ignatova, Z. (2011). Folding at the birth of the nascent chain: coordinating translation with co-translational folding. Curr. Opin. Struct. Biol. *21*, 25–31.

Zhang, Y., and Pelechano, V. (2021). High-throughput 5′P sequencing enables the study of degradation-associated ribosome stalls. Cell Reports Methods, 100001.

STAR★METHODS

KEY RESOURCES TABLE

REAGENT or RESOURCE	SOURCE	IDENTIFIER
Antibodies		
Monoclonal ANTI-FLAG® M2 antibody produced in mouse	Sigma	Cat# F3165; RRID: AB_259529
Monoclonal Anti-HA antibody produced in mouse, clone HA-7	Sigma	Cat# H3663; RRID: AB_262051
Anti-GFP from mouse IgG1κ (clones 7.1 and 13.1)	Roche	Cat# 11814460001; RRID: AB_390913
Monoclonal Anti-c-Myc antibody produced in mouse, clone 9E10	Sigma	Cat# M5546; RRID: AB_260581
Rabbit polyclonal anti-Not5	Oberholzer and Collart, 1998	N/A
Rabbit polyclonal anti-Egd2	Panasenko et al., 2006	N/A
Rabbit polyclonal anti-Caf40	Panasenko et al., 2006	N/A
DYKDDDDK Tag Monoclonal Antibody (FG4R), DyLight 650	Thermo Fischer (Invitrogen)	Cat# MA1-91878-D650; RRID: AB_2537623
Chemicals, peptides, and recombinant proteins		
3-indoleacetic acid	Sigma-Aldrich	Cat# I2886
Deposited data		
tRNA microarrays	This paper	GEO: GSE137567
Ribosome profiling (RiboSeq)	This paper	GEO: GSE137613
5′P-Seq	This paper	GEO: GSE168290
Mass spectrometry	This paper	Pride partner repository PXD021551 and PXD021580
Ensembl R64-1-1, build 84 - genome and gtf	Ensembl genome database project	http://ftp.ensembl.org/pub/release-84/
eif5A degron RiboSeq data	Associated GEO deposit; Schuller et al., 2017	GEO: GSE89704
rli1 degron and dom34 deletion, RiboSeq data	Associated GEO deposit; Guydosh and Green, 2014	GEO: GSE52968
rli1 degron RiboSeq data	Associated GEO deposit; Young et al., 2015	GEO: GSE69414
Code	This paper	https://zenodo.org/record/5150443
Experimental models: Organisms/strains		
BY4739 wild type	Euroscarf	MY3415
BY4739 *not4::KANMX4*	Euroscarf	MY3417
BY4739 *not5::KANMX4*	Euroscarf	MY3418
BY4742 wild type	Euroscarf	MY3672
BY4742 *not3::NATMX4*	This paper	MY10778
BY4742 *not4::NATMX4*	This paper	MY10776
BY4742 *not5::NATMX4*	This paper	MY5673
KY803 *gcn4Δ* wild type	Hope and Struhl, 1986	MY1
KY803 *gcn4Δ not3::URA3*	Oberholzer and Collart, 1998	MY508
KY803 *gcn4Δ not5-1*	Oberholzer and Collart, 1998	YOU123
KY803 *gcn4Δ not5-2*	Oberholzer and Collart, 1998	YOU142
rps7A_K4R	Toshifumi Inada; Ikeuchi et al., 2019	MY12303
RPS7A	Toshifumi Inada; Ikeuchi et al., 2019	MY12304
not5::NOT5-Taptag-URA3	Azzouz et al., 2009a	MY5321
not1::NOT1-GFP-TRP1	This paper	MY4073
not4::NOT4-GFP-TRP1	This paper	MY4076

(*Continued on next page*)

Continued

REAGENT or RESOURCE	SOURCE	IDENTIFIER
not5::NOT5-GFP-TRP1	This paper	MY4077
RP10	David Shore; Albert et al., 2019	RP10
not1::NOT1-9Myc-AID-NATMX4 ura3::ADH1p-TIR1-URA3	This paper	MY13517
Recombinant DNA: Plasmids		
p*NOT4*p-Myc$_6$-Not5$_{71-560}$-*CYC1*t-*URA3*	This paper	pMAC1271
p*NOT4*p-Myc$_6$-Not5$_{104-560}$-*CYC1*t-*URA3*	This paper	pMAC1272
yEPlac181-*HYP2*-Flag	Thomas Dever, PC3290; Saini et al., 2009	pE649
p*CUP1*p- HA$_7$-*RPT1-CYC1*t-*LEU2*	Panasenko et al., 2019	pOP108
p*CUP1*p-Flag-*rli1*-K16R-*LEU2*	This paper	pMAC1321
p*CUP1*p-Flag-*RLI1- CYC1*t-*LEU2*	This paper	pMAC1322
p*SPT3*p-HA$_7$-*NOT2- CYC1*t-*LEU2*	This paper	pMAC724
p*NOT4*p-Myc$_6$-*NOT4-CYC1*t-*LEU2*	Panasenko and Collart, 2011	pMAC906
p*NOT4*p-Myc$_6$-Not4$_{1-430}$- *CYC1*t-*LEU2*	Panasenko and Collart, 2011	pMAC907
p*NOT4*p-Myc$_6$-Not4$_{78-587}$-*CYC1*t-*LEU2*	Panasenko and Collart, 2011	pMAC908
pNAT-AID-9Myc	Morawska and Ulrich, 2013	Addgene, #99523
pBSSK-*rli1*-K16R	This paper	pMAC1314
p*SPT3*p-HA$_7$-*RLI1-CYC1*t-*LEU2*	This paper	pMAC1136
Software and algorithms		
cutadapt	Martin, 2011	https://cutadapt.readthedocs.io/en/stable/
HISAT2	Kim et al., 2015	http://daehwankimlab.github.io/hisat2/
ImageJ	Schneider et al., 2012	https://imagej.nih.gov/ij/
Bowtie2	Langmead and Salzberg, 2012	http://bowtie-bio.sourceforge.net/bowtie2/index.shtml
Samtools	Li et al., 2009	https://sourceforge.net/projects/samtools/
EdgeR	Robinson et al., 2010	https://bioconductor.org/packages/release/bioc/html/edgeR.html
riboWaltz	Lauria et al., 2018	https://github.com/LabTranslationalArchitectomics/riboWaltz
lmerTest	Kuznetsova et al., 2017	https://cran.r-project.org/web/packages/lmerTest

RESOURCE AVAILABILITY

Lead contact

Further information and requests for resources and reagents should be directed to, and will be fulfilled by, the lead contact (martine.collart@unige.ch).

Materials availability

All newly created plasmids or strains are available upon request from the lead contact.

Data and code availability

tRNA microarray data are accessible under the accession number GEO: GSE137567 in the Gene Expression Omnibus (GEO) database, RiboSeq of *not4Δ* and *not5Δ* under GEO: GSE137613, 5′P-Seq data under GEO: GSE168290, and the mass spectrometry data in the Pride partner repository under PXD021551 and PXD021580. All code used in the manuscript is available (https://zenodo.org/record/5150443).

Any additional information required to reanalyze the data reported in this paper is available from the lead contact upon request.

EXPERIMENTAL MODEL AND SUBJECT DETAILS

Budding yeast *S.cerevisiae* strains used in this manuscript were from either from Euroscarf and derived from BY4739 (*MATα his3 leu2 ura3 lys2*): wild-type (MY3415), *not4Δ* (MY3417, isogenic except *not4::KANMX4*) and *not5Δ* (MY3418, isogenic except

not5::KANMX4) used for ribosome profiling (RiboSeq), or the BY4742 background (*MATα his3Δ leu2Δ lys2Δ0 ura3Δ*), wild-type (MY3672), *not3Δ* (MY10778, isogenic except *not3::NATMX4*) *not4Δ* (MY10776, isogenic except *not4::NATMX4*) and *not5Δ* (MY5673, isogenic except *not5::NATMX4*) or they have been described previously: isogenenic to KY803 (Hope and Struhl, 1986) are *not3::URA3* (MY508, Collart and Struhl, 1994), *not5-1* (YOU123) and *not5-2* (YOU142) (Oberholzer and Collart, 1998) whereas Not5-TAP (MY5321) expresses Not5 fused to TAP, a double affinity tag composed of the calmodulin binding peptide followed by a TEV (Tobacco Etch Virus) protease cleavage site and the Protein A tag (Azzouz et al., 2009a). The strains expressing wild-type or K4R Rps7A were a kind gift from the Inada laboratory (Ikeuchi et al., 2019). The strains MY4073, MY4076 and MY4077 expressing respectively Not1, Not4 and Not5 fused to GFP were created by PCR (Longtine et al., 1998) in the KY803 background. The ΔN-Not5 derivatives (pMAC1271 and 1272) were created by the drag and drop method (Jansen et al., 2005) and verified by sequencing. The high copy eIF5A plasmid was a kind gift from T. Dever (PC3290). The plasmid expressing $Rli1_{K16R}$ was synthesized by Genecust. The mutated Lys codons are: 66, 118, 123, 130, 160, 167, 171, 183, 218, 223, 257, 405, 414, 420, 455 and 587. Wild-type and mutant Rli1 were then amplified by PCR with a forward primer including a Flag tag and a reverse primer, for cloning into pOP108 (Panasenko et al., 2019) with Not1 and Xho1 to make pMAC1322 and pMAC1321. Rli1 was also cloned behind the *SPT3* promoter by drag and drop cloning into pMAC724 to make pMAC1136 used for the ubiquitination assay. All clones were verified by sequencing. Not4 derivatives previously described (Panasenko and Collart, 2011) were subcloned by SacI and XhoI into pGREG424 (Jansen et al., 2005) to make pMAC906-908. The Not1 degron was created in strain YDR10 (kind gift from David Shore) and PCR amplification of 9Myc-NATMX4 with Not1 specific primers using plasmid pE641. The strain was verified by PCR. Not1 depletion was obtained by addition of auxin (3-indoleacetic acid, Sigma-Aldrich I2886, stock solution at 250 mM in EtOH) at 1mM final for 15 min to exponentially growing cells diluted to OD_{600} 0.3 after an overnight culture in glucose rich medium (YPD), when they reached OD_{600} 0.8. Equivalent amounts of EtOH 100% was added for the control. All experiments were performed with cells growing in YPD or in selective SC medium for experiments with cells transformed with one or more plasmids.

METHOD DETAILS

Ribosome profiling (RiboSeq)

RiboSeq (Ingolia, 2016, 2009) of *not5Δ* (MY3418) and *not4Δ* (MY3417) was performed in biological duplicates as described (Panasenko et al., 2019). Briefly, cells were grown to exponential phase, total extracts prepared in presence of CHX (0.1 mg/ml) were treated with RNase I, and monosomes were isolated after sucrose gradient separation. Libraries were made from the ribosome protected fragments and subjected to deep sequencing.

For the RiboSeq samples, all fastq files were adaptor stripped using cutadapt (Martin, 2011). Only trimmed reads were retained, with a minimum length of 20 and a quality cutoff of 2 (parameters: -a 10 CTGTAGGCACCATCAATAGATCGGAAGAGCACACGTCT GAACTCCAGTCAC–trimmed-only–minimum-length = 20–quality-cutoff = 2). Histograms were produced of ribosome footprint (RPF) lengths that were very homogeneous with highest reads between 28 and 31 that were kept for the analysis. Reads were mapped, using default parameters, with HISAT2 (Kim et al., 2015) to R64-1-1, using Ensembl release 84 gtf for transcript definitions. UTR definitions were taken from the *Saccharomyces* Genome Database and a standard region of 100bp was used where a gene's UTR was not defined. A minimum length of 30bp was implemented to ensure appropriate mapping around the start and stop codons. For the mapping, only unique alignments to transcripts were retained. A full set of 6692 CDSs were established for R64-1-1 Ensembl release 84 and extended by the same UTR sequences defined above. The filtered reads were then mapped to this transcriptome with bowtie2 (Langmead and Salzberg, 2012), using default parameters.

For all downstream analysis, dubious ORFs were filtered to leave 5929 transcripts. The A/P site position of each read was predicted by riboWaltz (Lauria et al., 2018) and aggregated over all transcripts. Metagene plots were generated for genes with a mean of $\log_2$ RPKM above 5 (2604 for wild-type and *not4Δ*, and 2849 for *not5Δ*). For the plots shown in Figure 1A, genes were filtered if shorter than 600bp to ensure that metagene at start and stop did not overlap. For the scaled plot, genes longer than 100 nucleotides were retained and split into 100 equal bins. This excluded only 2 RP mRNAs. Normalization was performed as described (Ingolia et al., 2009).

Codon frequency was defined for each gene as the number of each codon type divided by the total number of codons in the CDS. The ribosome dwelling occupancy (RDO) was defined by the read count for each codon type divided by the total counts for the CDS and normalized to codon frequency. Mean RDOs for a group of genes was calculated as the average value for each codon. Genes used in the analysis of RDO were restricted to those with RPKMs greater than 1 across all samples, leaving 5048 genes. The $\log_2$ ratio of *not4Δ* and *not5Δ* RDOs were taken relative to wild-type for each codon.

Where RDOs are reported for E, P, A sites, a count on a given codon is taken to be the number of E, P, A sites covering it, respectfully. Where RDOs are reported as being calculated n bases upstream of a given codon, A sites counts were generated for each codon occupying this position. The RDOs were then calculated from these counts, as in the previous paragraph. When reporting a pairwise correlation, RDO values for each codon were calculated for each sample and correlated across all 61 codons.

Optimal codons were defined as the 15 codons with the highest tRNA adaptation index (tAI) and non-optimal codons as the 15 with the lowest tAI from Pechmann and Frydman (2013). Differential expression was performed on the same set of genes (RPKM > 1) comparing wild-type and *not4Δ* or *not5Δ* duplicates using edgeR (Robinson et al., 2010) on default settings. Where correlations are reported, the Pearson method was used.

Published data on ribosome footprint alterations due to various deletions and degrons was downloaded and re-analyzed: *eIF5Ad* from Schuller et al. (2017), *rli1d* from Young et al. (2015), *dom34Δ* and *dom34Δ rli1d* from Guydosh and Green (2014). The same methods of mapping, filtering and analysis detailed above for *not4Δ* and *not5Δ* were recreated for all published data used, starting from raw fastq files.

To assess relative aminoacyl–tRNA charging levels for each cognate codon, where a codon is read by two tRNAs, charging was summed (weighted by its usage divided by the total codon usage of all codons read by each tRNA). Leu-TTA/G (fold change 0) was excluded through a Grubbs outlier test on charging fold changes ($p = 0.02956$).

RNA extraction and analysis

Total RNA was prepared either by the hot acid phenol method (Collart and Oliviero, 2001) or cells were lysed as for polysome profiling (Panasenko and Collart, 2012) without or with the addition of 200 mM 1,6-hexanediol and EDTA 25mM in the lysis buffer. For polysome profiling lysis, yeast in exponential growth phase were washed with cold water, and resuspended in buffer A (20 mM HEPES, pH8.0, 50 mM KCl, 10 mM $MgCl_2$, 1% Triton X-100, 1 mM DTT, 1 mM PMSF and protease inhibitor cocktail) with 100 μg ml^{-1} of CHX. Cells were broken with 0.5 mL of glass beads in 0.5 mL of buffer A for 15 min at 4°C. The lysates were clarified by centrifugation at 14000 g for 10 min. Total RNA from the lysate was then extracted by hot acid phenol. mRNA levels were measured by RT-qPCR. Briefly 1 μg of total RNA was DNased with RQ1 enzyme (Promega) and processed for reverse transcription using M-MLV reverse transcriptase (Promega) and random hexamer primers (Thermo Scientific). Specific cDNAs were amplified with specific primers (available upon request). Quantification of each tested cDNA was performed on a CFX96 Real-Time PCR Detection System (Biorad) with SensiFAST SYBR No-ROX Kit (Bioline). Biological triplicates were analyzed. For all three biological replicates (each with technical triplicates) in both wild-type and *not5Δ* strains, the difference in ΔCT was calculated between the different extraction procedures, but also *RPS1B*, *POM152* and *PUN1*, were normalized to *SED1* in wild-type and *not5Δ* respectively for comparison purposes. The resulting normalized ΔCT values (using *SED1* as a baseline) were then used as a dependent variable in fitting a mixed effects model with lmerTest (Kuznetsova et al., 2017). The strain (wild-type or *not5Δ*) was encoded as a fixed effect and the transcripts and technical duplicates as random effects. The resulting $p = 0.0451$ for the fixed effect coefficient showing the influence of the Not5 deletion indicates that normalized ΔCT is significantly lower in *not5Δ* than in wild-type. Results were similar whether 1-6 hexanediol was added together with EDTA or without any EDTA.

5′P-Seq

RNA was prepared from 50 mL of exponentially growing cells in YPD and treated or not with auxin. HT-5PSeq libraries were generated as reported (Zhang and Pelechano, 2021) with minor modifications. In brief, 15μg total RNA, containing 5% total RNA from *Schizosaccharomyces pombe* as spike-in, was used. Each sample was spited in two. One part was used for preparing conventional HT-5PSeq libraries and the other part for was random fragmented prior to the preparation of HT-5PSeq libraries (negative control).

For HT-5PSeq Libraries: 7.5 μg RNA was ligated over night at 16°C to r5P_RNA_MPX oligo (CrArCrGrArCrGrCrUrCrUrUrCrCrGrArUrCrU rXrXrXrXrXrX rNrNrNrNrNrNrN) carrying a sample barcode (rX) and unique molecular identifiers (rN). Ligase was deactivated using 5mM EDTA and heat at 65°C for 10 minutes (up to X individual barcoded RNA ligations were pooled) and subsequent purified using 1.8x volumes of RNAClean XP beads (Beckman Coulter). Ligated RNA was then reverse transcribed using random hexamer (5Pseq-RT, GTGACTGGAGTTCAGACGTGTGCTCTTCCGATCTNNNNNN, 20 μM) and oligo-dT (5Pseq-dT, GTGACTGGAGTTCAGACGTGTGCTCTTCCGATCTTTTTTTTTTT at 0.05 μM) oligos to prime. After, remaining RNA was degraded using NaOH. Ribosomal RNA was removed using previously described rRNA DNA oligo depletion mixes, following a duplex-specific nuclease (DSN, Evrogen) digestion. rRNA depleted cDNA was amplified by PCR (17 cycles) and final product was enriched for fragments with the range of 300-500 nt using Ampure XP.

Size selected HT-5P Libraries were quantified by fluorescence (Qubit, Thermo Fisher), size estimated using an Agilent Bioanalyzer and sequenced using a NextSeq500 Illumina sequencer (75 cycles High output kit).

Sequencing files were demultiplexed using bcl2fastq v2.20.0.422 (one mismatch, minimum length 35 nt), and adapters were trimmed using cutadapt 2.3. at default settings, allowing one mismatch and minimum read length of 35nt. In addition to standard illumine dual index (i5, i7), the inline sample and UMI barcode was analyzed using Umitools. Reads were mapped to the concatenated genome of *S. cerevisiae* (R64-1-1) and *S. pombe* (ASM294v2) using STAR.

Second read enables to splits reads between oligo-dT or random primer. That information was not used in the current analysis.

To calculate 5′P-Seq pausing scores, equivalent to A-site RDO, the mean depth was calculated 17 nt upstream of each codon type in each deletion or degron strain and the log ratio was taken with the corresponding wild-type.

In vivo ubiquitination assay

The assay was performed as previously described (Panasenko et al., 2006) with cells expressing His_6-ubiquitin under the control of the *CUP1* promoter and ubiquitinated proteins were purified by nickel affinity chromatography. Cells were grown in medium containing 0.1 mM $CuSO_4$ and 50 OD_{600} units were collected at OD_{600} below 2.0. Cell pellets were weighed and resuspended in G-buffer (100 mm sodium P_i, pH 8.0, 10 mm Tris-HCl, 6 m guanidium chloride, 5 mm imidazole, 0.1% Triton X-100) to 50 mg/ml. 1 mL of cell suspension was disrupted with 0.6 mL of glass beads during 6 min at 4°C and spun for 20 min at 13000 × *g*. To remove guanidium chloride, 20 μL of the supernatants were diluted in 1.2 mL of water and concentrated with Strataclean resin (Stratagene)

and eluted with 50 μL of Laemmli SB. 3–5 μL of TE were kept for analysis. The rest of the supernatant was incubated with 30 μL of nickel-nitrilotriacetic acid-agarose (QIAGEN) for 2 h at room temperature with mild rotation. The agarose beads were washed 3 times with 0.5 mL of U-buffer (100 mm sodium P_i, pH 6.8, 10 mm Tris-HCl, 8 m urea, 0.1% Triton X-100). His_6-ubiquitinated proteins were eluted with 50 μL of 2 × Laemmli SB and 12–15 μL of samples were analyzed by western blot with the relevant antibodies.

Immunofluorescence

Cell expressing Not1-, Not4- and Not5-GFP were used for localization experiments. A total of 10 mL of exponentially growing yeast were fixed with 600 μL of 4% paraformaldehyde solution at room temperature (RT) for 1 h. The cells were collected and the pellet was washed twice with phosphate buffered saline (PBS) containing 0.1% tween-20. Cells were resuspended in 1 mL of spheroplasting buffer (0.1 potassium phosphate pH 7.4, 1.2 M sorbitol) and treated with 10 μL of 5 mg/ml zymolase 20T (USBiological) for 30 min at 30˚C. After washing with spheroplasting buffer, the spheroplasts suspension was blocked with PBS containing 0.1% BSA, 30 min at RT. DAPI (Sigma) was used to mark the nucleus and samples were covered with mounting solution (ProLong™ Diamond Antifade Mountant, ThermoFisher). For cells expressing Flag-eIF5A they were incubated overnight with the primary antibody at a final concentration of 5 mg/μl in 1X PBS and washed with PBS containing 2% BSA. Images were taken using a Confocal Laser Scanning Microscopy (LSM 800 Zeiss) and obtained by optical sectioning (z stacks) with a step size of 0.40 μm and further processed with ImageJ. Alternatively they were taken using a Widefield Microscope (Axiocam Fluo) and then processes with ImageJ. For the co-staining of Not5-GFP and Flag-eIF5A at least 9 fields with an average of 5-19 double stained cells were analyzed.

FRAP

After dilution of a day culture, cells (MY4077) were grown in 5 mL of YPD to reach OD_{600} of 0.8 in the morning. 1 mL of the culture was spun in a microfuge and resuspended in 50 μL of SC-TRP medium. 10 μL of this cell suspension was added on top of 1.5% agar pad prepared in -TRP already on a coverslip. Live images were taken with a Nikon A1r spectral microscope. The crucial aspect is to have the cells growing in contact with an agar pad in order to provide ideal conditions for their growth at least for 1–2 h, until the agar pad is dry (immobilizing cells between agarose and a coverslip does not flatten or distort cells, while coverslip pressure on a glass slide does). Note that in order to reduce the background signal and have a good signal/noise ratio, it is essential to image the cells in synthetic media (e.g., –TRP); this applies to both the media in which the cells are suspended on the coverslips as well as to the agar pad.

The data analysis (Xing et al., 2020) and interpretation (Kroschwald et al., 2018; Reits and Neefjes, 2001; Xing et al., 2020) was carried out as described by others, with minor modifications to adapt to our experimental conditions. The images were processed using ImageJ 1.53c and we calculated the corrected recovered intensities of the bleached area from 4 different variables (see below), where we first substracted the background fluorescence from each. We measured: the average fluorescence intensities at each time point in the bleached area during the recovery phase (1); the intensities from the bleached cell's cytoplasm, excluding the bleached area before (2) and with one interval after (3) bleaching; the intensities from an un-bleached cell's cytoplasm in each time point as a reference (4). Then the corrected intensities during recovery were normalized for the area's pre-bleaching intensities measured from 3 different time points before the bleaching. The normalized values were fitted to a single exponential recovery curve. According to this we obtained the informative values, which describe the kinetics/dynamics of the fluorescent signal related to the Not5 condensates after photobleaching (K: exchange rate of fluorescence) and ($t_{1/2}$: half-time of recovery).

To visualize the dynamics of Not condensates, we chose different time points from our FRAP series (before bleaching, just after bleaching and at 5, 25 and 140 s during the recovery phase). The images were cropped to the photobleached cell. After subtracting the background fluorescence defined by zones with no detectable condensates and setting it as default for each time point stack, we were able to visualize the punctate staining (condensates). To highlight them, we applied the ImageJ's maximum filter option for post-processing. By this, each pixel was set to a certain value automatically, calculated as a grayscale dilation, also considering the values of the neigbouring pixels. To illustrate changes in fluorescence intensity, a pseudocolor assignment (rainbow RGB) was used, where the color corresponds to the intensity as it is marked on the calibration bar.

Protein aggregate analysis

Protein aggregates were isolated as described previously (Panasenko and Collart, 2012). Briefly, 50 OD_{600} units of logarithmically growing cells in YPD were harvested and resuspended in lysis buffer (20 mM Na-phosphate, pH 6.8, 10 mM DTT, 1 mM EDTA, 0.1% Tween 20, 1 mM PMSF, protease inhibitor cocktail, 3 mg ml^{-1} zymolyase T20) and incubated at 30°C for 20 min. Chilled samples were sonicated (3 times 10 s at duty cycle 40%) and centrifuged for 20 min at 200 g at 4°C. Supernatants were adjusted to an identical protein concentration of 5.0 mg ml^{-1}. 500 μl of supernatants were centrifuged at 16000 g for 20 min at 4°C to pellet the aggregated proteins. After removing supernatants, aggregated proteins were washed twice with washing buffer (20 mM Na-phosphate, pH 6.8, 1 mM PMSF, protease inhibitor cocktail) containing 2% NP-40, sonicated (10 s at duty cycle 40%), and centrifuged at 16000 g for 20 min at 4°C. Aggregated proteins were washed in washing buffer (sonication, 10 s at duty cycle 40%). A proteomic analysis performed by LC-MS at the core facility of the Faculty of Medicine (University of Geneva).

tRNA microarrays

To determine the fraction of charged tRNAs we followed the procedure described in Kirchner et al. (2017). Briefly, total RNA was isolated in mild acidic conditions (pH 4.5) which preserves the aminoacyl-moiety. Each sample was split into two aliquots and one was

oxidized with periodate to which the changed tRNAs remain intact and following subsequent deacylation (100 mM Tris (pH 9.0) at 37°C for 45 min) was hybridized to Cy3-labeled RNA/DNA stem-loop oligonucleotide. The second aliquot was deacylated to receive the total tRNA and hybridized to Atto647-labeled RNA/DNA stem-loop oligonucleotide. Both aliquots were analyzed on the same tRNA microarrays with tRNA probes covering the full-length sequence of cytoplasmic tRNA species as described previously.

For tRNA abundance, total RNA was isolated at alkaline pH to simultaneously deacylate all tRNAs. tRNAs labeled with Cy3-labeled RNA/DNA stem-loop oligonucleotide were hybridized on the same microarray with tRNAs isolated from wild-type strain and labeled with Att647-labeled RNA/DNA stem-loop oligonucleotide. The arrays were normalized to spike-in standards, processed and quantified with in-house python scripts.

Tandem affinity purification

Not5-TAP was purified by tandem-affinity purification, first by IgG Sepharose then by calmodulin affinity as described (Azzouz et al., 2009a). 20 l of cells were grown to an OD_{600} of 2 to 3. Cells were spun for 10 min at 5000 g at 4°C, and then the pellets were washed with 1 l of cold E buffer (20 mM HEPES, pH 8, 350 mM NaCl, 0.1% Tween 20, 10% glycerol) and spun for 10 min at 5000 g at 4°C. The final pellets were resuspended in 50 mL of cold E buffer completed with protease inhibitors. 50 mL of cell suspension was broken eight times during 30 s using a Bead Beater filled up to one-third of the volume with glass beads. Cell lysates were spun for 10 min at 5000 g at 4°C. The extracts were clarified for 45 min at 43000 rpm at 4°C, and the protein concentration of the supernatants was measured by the Bradford assay. 2 g of proteins was used for purification over 400 μL of an immunoglobulin G-Sepharose column (IgG Sepharose Fast Flow; Pharmacia). After 2 h of protein binding with rotation at 4°C, the column was washed with 10 mL of E buffer and 10 mL of tobacco etch virus (TEV) protease cleavage buffer (10 mM Tris-HCl, pH 8, 150 mM NaCl, 0.5 mM EDTA, 0.1% Tween). TEV protease (100 U) cleavage was performed in 1 mL buffer at 18°C for 2 h. The TEV eluate was bound to 100 μL of calmodulin affinity resin (Stratagene) in 3.6 mL of calmodulin binding buffer (10 mM Tris-HCl, pH 8, 150 mM NaCl, 1 mM Mg acetate, 1 mM imidazole, 10 mM $CaCl_2$, 0.1% Tween, 10% glycerol) by rotating for 1 h at RT. The column was washed with 10 mL of calmodulin binding buffer, and bound proteins were recovered in three elutions using calmodulin elution buffer (10 mM Tris-HCl, pH 8, 150 mM NaCl, 1 mM magnesium acetate, 1 mM imidazole, 10 mM EGTA, 0.1% Tween, 10% glycerol). Co-purifying proteins were identified by LC-MS.

Immunoprecipitation and affinity purification

To purify nascent chains, Flag-tagged Rpt1 derivatives were induced from a plasmid with stalling sequence (pOP164; Panasenko et al., 2019) by 10 min of copper treatment and a total of 100 OD_{600} units of cells were broken with 0.3 ml of glass beads in 0.4 ml of lysis buffer (20 mM HEPES, pH 7.5, 20 mM KCl, 10 mM $MgCl_2$, 0.1% Triton X-100, 1 mM DTT, 1 mM PMSF and a protease inhibitor cocktail) for 15 min at 4 °C. After clarification cell lysates were treated with 1.6 μL of 10 mg/ml RNaseA added to 400 μL of total extract and incubated for 5 min at RT. Treated extracts were fractionated in sucrose gradients as described before (Panasenko and Collart, 2012). Heavy fractions from the sucrose gradient were incubated with anti-Flag antibodies prebound to protein G magnetic beads. Anti-Myc prebound beads were used as a negative control.

SILAC

For stable isotope labeling by amino acids in cell culture (SILAC) experiments wild-type and *not4Δ* cells in triplicates were grown until saturation overnight in SC-complete medium (2% glucose) containing not labeled or "light" L-lysine ($^{12}C_6$, $^{14}N_2$). Next day the samples were diluted to an OD_{600} of 0.1-0.2 and grown for 3 h in SC-complete medium with light lysine. The cells were then shifted to medium containing labeled or "heavy" L-lysine ($^{13}C_6$, $^{15}N_2$) (Silantes) and were grown for another 3 h, harvested and analyzed by LC/MS as described previously (Hughes et al., 2014, 2019).

Briefly, for lysis, cell pellets were reconstituted in 100 mM HEPES pH 7.3 containing 4% SDS, 10 mM dithiothreitol, and 0.5X cOmplete protease inhibitor (Sigma) and transferred to lysing matrix Y tubes (MP Biomedicals). Samples were disrupted on a FastPrep 5G instrument (6M/s, 45 s, 2 cycles). Lysed samples were incubated at +60°C for 30 min and then chloroacetamide was added to a final concentration of 40 mM. After a 30 min incubation in the dark at room temperature (+24°C), samples were quenched by addition of dithiothreitol to a final concentration of 40 mM. For clean-up prior to digestion, samples were prepared using SP3 in standard conditions as described previously (Hughes et al., 2014, 2019). Cleaned proteins were subject to proteolysis using trypsin and rLysC (Promega) and digested at +37°C for 18 hs.

After tryptic digestion, samples were centrifuged at 10000 g for 30 s and peptide-containing supernatant recovered using a magnetic rack. Samples were then tandem mass tag (TMT) labeled using 6-plex reagents (Thermo Scientific) as described previously (Hughes et al., 2016). Briefly, reconstituted TMT label (10μg/μL) was added to each peptide sample at a concentration ratio of 2:1 (μg:μg TMT label to peptide) and incubated at room temperature for 30 min. An additional aliquot of the TMT was then added (4:1 final ratio) and incubated for a further 30 min. For TMT layout, wild-type sample replicates were in channels 126 – 128, with mutant samples in 129 – 131. Individually labeled samples were combined and concentrated in a SpeedVac centrifuge and then desalted using SepPak cartridges (50 mg t-C18 material, Waters). Briefly, columns were rinsed twice with acetonitrile (+0.1% TFA) and twice with water (+0.1% TFA). After sample loading, cartridges were rinsed twice with water (+0.1% formic acid, FA) and then eluted with 80% acetonitrile (+0.1% FA). After clean-up, peptides were fractionated using high-pH reversed phase chromatography with fraction concatenation as described previously (Hughes et al., 2016). A final set of 12 fractions was desalted prior to MS analysis

using StageTips (3-disc plug, C18 Empore material, 3M). Eluted peptides were concentrated to dryness using a SpeedVac centrifuge (Thermo Scientific) and subsequently reconstituted in 1% formic acid.

Analysis of peptide samples was carried out on an Orbitrap Fusion MS system (Thermo Scientific). Specifically, peptide samples were initially injected and chromatographically separated using an Easy nLC 1000 system (Thermo Scientific) with a trapping-analytical column setup. Trapping columns were packed in 75μm internal diameter capillaries to a length of 3 cm with 1.9 μm Reprosil-Pur C18 beads (Dr. Maisch). Trap columns were packed in-house in fritted capillaries prepared with a combination of formamide and Kasil (1:3 ratio). Gradient elution of peptides was performed on a C18 (Reprosil-Pur, 1.9 μm C18, Dr. Maisch) analytical column packed to a length of 25 cm in a 75 μm internal diameter capillary with a nanospray tip (New Objective). The analytical column was heated to 50°C using an AgileSLEEVE oven (Analytical Sales & Service) and eluted across a 120-min gradient of acetonitrile (+0.1% FA) (20-min column rinsing and 20 min injection overhead for a total run time per injection of 160-min) at a flow rate of 350 nL/min.

Data acquisition on the Orbitrap Fusion was carried out using a data-dependent tandem MS/MS (MS2) method with synchronous precursor selection MS/MS/MS (SPS-MS3) detection of TMT reporter ions. Survey scans (MS1) covering the mass range of 380 – 1500 m/z were acquired at a resolution of 120000 (at m/z 200), with quadrupole isolation enabled, an S-Lens RF level of 60%, a maximum fill time of 50 millisec and an automatic gain control (AGC) target value of 4e5. For MS2 identification scan triggering, monoisotopic precursor selection was enabled, charge state filtering of 2 – 5, and dynamic exclusion of previously selected masses for 30 s (10ppm mass threshold). MS2 scans were acquired in the ion trap with the Turbo scan mode after CID fragmentation, a maximum fill time of 50 ms, an isolation window of 2 m/z, collision energy of 35%, and an AGC target of 1e4. Fragments for MS3 scans were selected based on a range of 400 – 1200 m/z, precursor ion exclusion (20 ppm high, 5 ppm low), and isobaric tag exclusion set to TMT. MS3 scans covering the mass range of 110 – 750 m/z were acquired at a resolution of 60000 in the Orbitrap after HCD fragmentation, a maximum fill time of 120ms, an isolation window of 2 m/z, collision energy of 65%, and an AGC target of 1e5. The total allowable cycle time was set to 3 s. MS2 and MS3 scans were acquired in centroid format, with MS1 in profile mode.

Acquired MS data were processed using Proteome Discoverer (version 2.1.0.62) as described previously (Hughes et al., 2016). Search engine parameters were specified as: trypsin enzyme, 2 missed cleavages allowed, precursor mass tolerance of 20 ppm, and a fragment mass tolerance of 0.8 Da. Carbamidomethylation of cysteine and TMT-6plex of the peptide N terminus were set as fixed modifications. Oxidation of methionine, TMT-6plex of lysine, and TMT 6-plex of lysine + 8 (for SILAC) were set as variable modifications. MS2 spectra were searched against the UniProt human proteome database (version 2016Jan) appended to a list of common contaminants. Peptide spectral match error rates were determined using the target-decoy strategy coupled to Percolator modeling of positive and false matches. Reporter ions were quantified from MS3 scans using an integration tolerance of 20 ppm with the most confident centroid setting. Output quantification values represented the signal-to-noise of the TMT value relative to the Orbitrap preamplifier. Data were filtered at the peptide spectral match-level to control for false discoveries using a q-value cutoff of 0.05 as determined by Percolator. The mass spectrometry proteomics data have been deposited to the ProteomeXchange Consortium (http://proteomecentral.proteomexchange.org) via the PRIDE partner repository (Vizcaíno et al., 2016) with the dataset identifier PXD021551.

Metabolomics

10 mL of yeast cells grown in glucose rich medium to exponential phase were collected and resuspended in 40 mL cold 0.9% NaCl (combining washing and quenching: the cold NaCl solution should stop effectively the metabolism and avoid leakage of intracellular metabolites into the medium; Dietmair et al., 2010). After centrifugation, 500 μl of extraction reagent (50% Acetonitrile (ACN), stored by −20°C) were added to the pellet, vortexed for 1 min, and spun at 14000 rpm for 10 min at 4°C. The supernatant was transferred to a clean vial and 500 μl extraction reagent was added again to the pellet, vortexed 1 min, spun at 14000 rpm for 10 min, and the new supernatant was added to the previously stored supernatant. The combined supernatants were finally freeze-dried (lyophilized) and sent for analysis to the Helmholz for Environmental Research, Leipzig, Germany.

QUANTIFICATION AND STATISTICAL ANALYSIS

Reported correlations were the Pearson's product-moment correlation coefficient and were used as test statistics to generate the associated p value by t test. All correlations and correlation tests were performed on groups of at least 30 in size. Enrichment of gene sets is defined via FDR after Benjamini-Hochberg adjustment from p values generated using a hypergeometric test. All t tests were performed on sample sizes of 30 or higher, where the central limit theorem applies regarding the normality assumption. We use Welch's t test in all cases, rather than the Student's t test, resulting in more conservative *p-value*, which is more reliable where variances and sample sizes are unequal. In one case, we used a Wilcoxon rank sum test (Wilcoxon, 1946) to compare two samples as a non-parametric proxy for a t test, so as to avoid any possible breach of the normality distribution assumption, since one of the samples had a size of 15. Proportion tests are performed with a two-sample test for equality of proportions using the Chi-square distribution with a Yates continuity correction to obtain a more conservative *p-value*.